Global theory of steady deep-cellular growth in directional solidification

Yong-Qiang Chen*
Department of Fundamental Subject, Tianjin Institute of Urban Construction, Tianjin 300384, China; School of Mathematical Science, Nankai University, Tianjin 300071, China

Jian-Jun Xu†
Department of Mathematics and Statistics, McGill University, Montreal, Quebec, Canada H3A 2K6; School of Material Science and Engineering, University of Science and Technology in Beijing, Beijing 100083, China; School of Mathematical Science, Nankai University, Tianjin 300071, China

(Received 9 October 2010; published 5 April 2011)

The present paper is concerned with the global asymptotic theory of steady deep-cellular growth in directional solidification of binary mixtures. We consider the two-dimensional model with nonzero isotropic surface tension and obtain the global uniformly valid asymptotic solutions for the steady state of the system in the limit of the Péclet number $\epsilon \to 0$; ϵ is defined as the ratio of the radius of the cell's tip and mass diffusion length. The whole physical space is divided into the outer region and root region; the solutions in each subregion are solved, respectively, and matched with each other in the intermediate region. The results show that given growth conditions and material properties, the global solutions for steady state of the system contain two free parameters: the Péclet number and asymptotic width parameter λ_0, which are related to the geometry of cellular structure: the cell tip radius and primary spacing. One of the most important conclusions drawn from this analysis is that the steady-state solutions of cellular growth have a complicated structure with three internal layers in the root region; for given (ϵ,λ_0), there exists a discrete set of the global steady-state solutions subject to the quantization condition that are profoundly affected by the surface tension. Each eigenvalue calculated from this quantization condition determines the total length of the finger described by the corresponding global steady-state solution.

DOI: 10.1103/PhysRevE.83.041601 PACS number(s): 81.10.Aj, 81.30.Fb, 05.65.+b, 47.54.−r

I. INTRODUCTION

Deep-cellular growth in directional solidification is a classic and fundamental subject in condensed matter physics and material science (Refs. [1–11]). It has been also a center of research activities on pattern formation and transition in the broad areas of nonlinear science as well as applied mathematics (Refs. [12–29]) for decades.

The typical experimental device used in directional solidification of a supersaturated, binary mixture is a Hele-Shaw cell. The system consists of a thin sample material and two uniform temperature zones: a hot zone with a temperature T_H higher than the melting temperature T_{M0} of a flat interface and a cold zone with a temperature T_C lower than the melting temperature. The sample is pulled at a constant speed V along the direction from the hot zone to cold zone.

Experimental results show that when the pulling speed V is sufficiently small, the interface will be flat, located at somewhere between the two zones. When the pulling speed increases beyond a critical number V_c, the flat interface becomes unstable due to the Mullins–Sekerka instability [2,3]. The studies of pattern formation on a planar interface near the critical number V_c has been an important subject in the material science community in the past few years [8,11], which is now well described by the weakly nonlinear theory.

When the pulling speed increases further, the interface pattern continuously evolves and eventually forms a steady deep-cellular structure. The fingers are aligned periodically with equal primary spacing ℓ_w (see Fig. 1). The cellular array may be transformed to a dendritic array as the pulling speed is larger than another critical number.

The whole pattern-formation process and its correlation with the operating conditions are very complicated in the regime $V \gg V_c$ because the problem becomes strongly nonlinear. One of most important issues for applications in the industries of material processing is to determine the steady states of the system at the late stage of growth. There have been many experimental investigations and numerical simulations on this subject during the last few decades (readers interested in those researches are referred to Refs. [11–13] and the literature quoted therein). The subject has been studied analytically for decades by a number of researchers in the field, such as Pelcé and Pumir [4], Weeks and co-workers [5,7], Caroli, Caroli, and Roulet [8], David [9], Billia and Trivedi [11,12], Karma [14,15], etc. However, the analytical solutions obtained so far all failed in the root region. Accordingly, these works cannot determine the global interface shape of cell, the locations of the cell's tip and bottom of the root, the total length of the cell, the concentrations of the impurity at the cell's tip and bottom, and, in particular, the mathematical relationships between all these important quantities and the operating conditions. There are also many numerical works (see, for instance, Refs. [16–18]) in the literature in recent years, which may show the global patterns of cellular array, but they cannot explore the properties of the singularities of the system at the bottom of the root, nor provide the mechanisms at work. Most recently, Pocheau and Georgrli attempted to determine the global shapes of interface from the tip to deep groove for the two-dimensional (2D) system of cellular growth under different growth conditions and materials [19,20]. They conducted a sequence of new

*yonqiang@gmail.com
†xu@math.mcgill.ca

 ©2011 American Physical Society

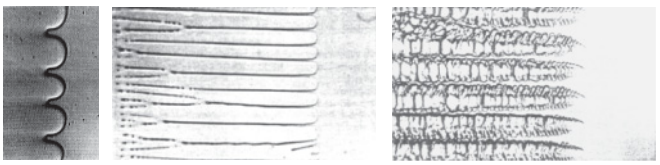

(a) (b) (c)

FIG. 1. Typical experimental photos of cellular and dendritic array growth in directional solidification with increasing pulling velocity V: (a) shallow cellular, (b) deep-cellular array, (c) dendritic array (see Ref. [11]).

careful experimental works and derived several experience formulas, as no relevant theoretical formula is available. Their formulas may satisfy some practical needs of determining the interface shape geometry, but these still cannot be applied all the way to the bottom of groove to determine the total length of cell. Moreover, these formulas do not lead to an understanding of the formation mechanism of global interface shapes. Hence, the problem remains.

The present paper is devoted to the theoretical investigation of steady deep-cellular array growth and attempts to determine the global interface shape from the cell tip to the bottom of the root. We consider the 2D model with small Péclet number ϵ defined as the ratio of the cell tip radius and mass diffusion length and nonzero isotropic surface tension. This case is quite practical, and the assumption of $\epsilon \ll 1$ can be well justified by the experimental data $\varepsilon = 0.02 - 0.14$ (refer to the experiments conducted by Somboonsuk *et al.* for the system succinonitrile-acetone in [12,13]). We obtain the global uniformly valid asymptotic solution for the steady state in the limit $\epsilon \to 0$.

Our results yield infinitely many global steady-state solutions of arrayed cellular growth with two free parameters: the Péclet number and asymptotic width parameter λ_0 under given growth conditions and material properties. These two parameters are related to the geometry of cellular structure, the tip radius, and primary spacing. It is found that the global steady-state solutions have a complicated structure of three internal layers in the root region and are subjected to a quantization condition substantially affected by the surface tension. The eigenvalue determined by such quantization condition yields the cell's full length of the corresponding global steady state.

The present paper is arranged as follows. In Sec. II, we give the mathematical formulation of directional solidification from a binary mixture; in sec. III, we introduce a curvilinear coordinate system (ξ,η) based on the classic steady finger solution [4,10], and formulate the cellular growth in such a coordinate system; in Sec. IV, we derive the outer solution in the region away from the bottom of the root (see Fig. 2), which is composed of the two parts: the regular perturbation expansion and the singular perturbation expansion. We further conduct the numerical calculations for the outer solutions derived in some typical cases and compare them with the available experimental results; in Sec. V, we divide the root region into three subregions and derive the inner solutions in each. By matching these inner solutions with each other and with the outer solution in the intermediate regions, we derive the composite global asymptotic solutions and show

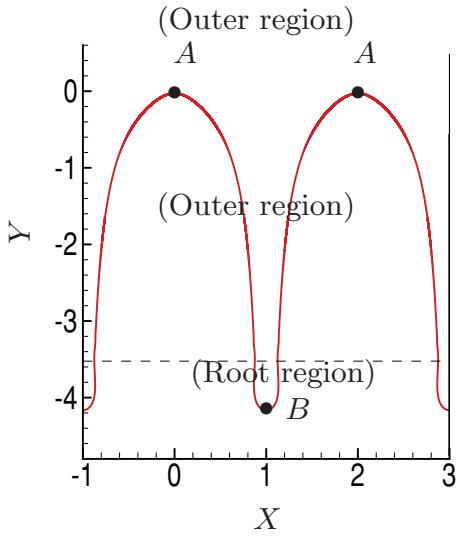

FIG. 2. (Color online) A sketch of cellular-array interface. (a) The cell tip; (b) the bottom of the root.

the numerical results of the solution for some typical cases. Finally in Sec. VI, we give conclusions and discussion.

II. MATHEMATICAL FORMULATION OF UNIDIRECTIONAL SOLIDIFICATION FROM A BINARY MIXTURE

We consider 2D dynamics in the Hele-Shaw cell by using the one-sided model. The temperature field is considered as prescribed. As usual, for the sake of simplicity we assume that the temperature in the region where an interfacial microstructure forms is linear with given gradient $(G)_{\rm D}$; the minor species in this binary-mixture system, considered as an impurity, is dilute; the solute diffusion in the solid phase is negligible; the thermodynamic properties other than the diffusivity are the same for both solid and liquid phases, and there is no convection in the system.

The solute-diffusion length in the system is defined as $\ell_{\rm D} = \kappa_{\rm D}/V$, where $\kappa_{\rm D}$ is the solute diffusivity. We use the tip radius $\ell_{\rm t}$ as the length scale and assume that $\ell_{\rm t} \ll \ell_{\rm D}$. The pulling speed V is used as the velocity scale, and $\ell_{\rm t}/V$ is used as the timescale. The scales of the temperature T and concentration C are set as $\Delta H/(c_{\rm p}\rho)$ and C_∞, respectively. Herein ΔH is the latent heat release per unit of volume of the solid phase, $c_{\rm p}$ is the specific heat, ρ is the density of the melt, and C_∞ is the impurity concentration in the far field. One may define the following dimensionless parameters: the Péclet number, $\epsilon = \ell_{\rm t}/\ell_{\rm D}$; the morphological parameter, $\mathbb{M} = -\frac{mC_\infty}{\Delta H/(c_{\rm p}\rho)}$, where $m < 0$ is the slope of the liquidus in the phase diagram; the surface-tension parameter, $\Gamma = \frac{\ell_{\rm c}}{\ell_{\rm t}} = \frac{\ell_{\rm c}\ell_{\rm D}}{\ell_{\rm t}^2}\frac{\ell_{\rm t}}{\ell_{\rm D}}$, where $\ell_{\rm c}$ is the capillary length defined as $\ell_{\rm c} = \gamma c_{\rm p}\rho T_{\rm M0}/(\Delta H)^2$, and γ is the surface-tension coefficient; the dimensionless gradient of the temperature, $G = \frac{\ell_{\rm D}}{\Delta H/(c_{\rm p}\rho)}(G)_{\rm D}$; the ratio of two length scales, $\lambda_{\rm G} = \ell_{\rm D}/\ell_{\rm G} = G/\mathbb{M}$, where $\ell_{\rm G} = -mC_\infty/(G)_{\rm D}$; the primary spacing parameter, $W = \ell_w/\ell_{\rm t}$. In most practical cases, the surface-tension parameter is very small, $\Gamma \ll 1$. We assume $\epsilon \ll 1$ and $\Gamma = O(\epsilon^2)$ and, accordingly, set $\Gamma = \epsilon^2\hat{\Gamma}$, where $\hat{\Gamma} = O(1)$.

Due to the periodicity of the solution, one may only consider a single cell. In this case the problem is equivalent to finger-like crystal growth in a channel with fixed side walls $x = \pm W$. For the case of arrayed-cellular growth, of course, W is a free parameter describing half of the primary spacing.

III. MATHEMATICAL FORMULATION OF THE PROBLEM IN A CURVILINEAR COORDINATE SYSTEM (ξ,η)

Assume that the origin of rectangular coordinates (x,y) is located at the cell tip; the temperature distribution in the growth zone is given by $T = \epsilon G(y - y_0)$. Thus, at $y = y_0$, one has the melting temperature $T = 0$, whose location in the device can be measured. With this setting, the value of parameter y_0, which determines the location of the system origin or cell tip, is a unknown quantity. Other unknowns of the problem are the concentration field C and the interface shape. The concentration field is governed by the solute diffusion equation and coupled with the known temperature field by the Gibbs-Thomson condition imposed at the interface.

In the present work, we shall utilize a moving frame fixed at the cell tip and adopt the curvilinear coordinate system associated with the Saffman-Taylor (ST) solution (see Refs. [26–31]). The reasoning for doing this is that though the global shape of cellular array may substantially differ from the ST finger shape in the physical plane (x,y), as is well known, the global shape of cellular array, however, is just a small perturbation near the ST finger shape in the (ξ,η) plane.

The stream and potential function of Hele-Shaw flow are denoted by $\Psi(X,Y)$ and $\Phi(X,Y)$, respectively. Let $\xi = -\Psi, \eta = \Phi, \zeta = \xi + \mathrm{i}\eta$. The ST solution can be expressed by the following mapping function:

$$Z = X + \mathrm{i}Y = Z(\zeta) = \lambda_0\zeta + \mathrm{i}\frac{2(1-\lambda_0)}{\pi}\ln\cos\left(\frac{\pi\zeta}{2}\right). \quad (1)$$

So we have

$$\begin{aligned} X(\xi,\eta) &= \xi - \frac{2(1-\lambda_0)}{\pi}\Theta, \\ Y(\xi,\eta) &= (2\lambda_0 - 1)\eta + \frac{(1-\lambda_0)}{\pi}\ln\left(\frac{\mathcal{R}}{4}\right), \end{aligned} \quad (2)$$

where λ_0 is the asymptotic width parameter relative to the primary spacing parameter W, $\Theta = \tan^{-1}\{\sin(\pi\xi)/[\cos(\pi\xi) + e^{\pi\eta}]\}$, and $\mathcal{R} = (e^{\pi\eta} - 1)^2 + 2e^{\pi\eta}[1 + \cos(\pi\xi)]$.

The variables $\{\xi = \xi(X,Y); \eta = \eta(X,Y)\}$ constitute a new orthogonal curvilinear coordinate system on the (X,Y) plane as shown in Fig. 3, where $x = WX(\xi,\eta), y = WY(\xi,\eta)$. In the curvilinear coordinate system (ξ,η), the linear distribution of temperature field is described by $T_B = \epsilon G[WY(\xi,\eta) - y_0]$. The basic steady state of cellular growth $\{C_B,\eta_B\}$ is subject to the governing equation:

$$\frac{\partial^2 C_B}{\partial\xi^2} + \frac{\partial^2 C_B}{\partial\eta^2} + \epsilon W\left(Y_\xi\frac{\partial C_B}{\partial\xi} + X_\xi\frac{\partial C_B}{\partial\eta}\right) = 0\,, \quad (3)$$

with the following boundary conditions:

(1) In the upstream far field: Away from cell tips, the effect of microstructure at the interface on the concentration distribution field is negligible. So the solution should reduce to that of a one-dimensional mass diffusion equation without a mass source in the field. Hence, it is posed that as $\eta \to \infty$, $C_B \sim 1 + Q_0(\epsilon)e^{-\epsilon W\eta}$, where $Q_0(\epsilon)$ is a constant, independent of the variables ξ,η.

(2) At the side walls, $\xi = \pm 1$: $\frac{\partial C_B}{\partial\xi} = 0$.

(3) At the interface $\eta = \eta_B(\xi,\epsilon)$:

$$C_B = y_* - \epsilon\lambda_G W Y(\xi,\eta) - \frac{\epsilon^2\hat{\Gamma}}{\mathbb{M}W}\mathcal{K}[\eta_B(\xi,\epsilon)]\,, \quad (4)$$

$$\frac{\partial C_B}{\partial\eta} - \eta_B'\frac{\partial C_B}{\partial\xi} - \epsilon W(1-\kappa)C_B(Y_\xi\eta_B' - Y_\eta) = 0, \quad (5)$$

where $\mathcal{K}\{\eta_B(\xi,\epsilon)\}$ is the twice mean curvature operator, and we designate that $\mathcal{K} > 0$, when an interfacial finger points to liquid phase side, and κ is the segregation coefficient. We denote that $y_* = \epsilon\lambda_G y_0$, and assume that $y_* = y_{*0} + \epsilon y_{*1} + \cdots$, as $\epsilon \to 0$.

(4) At the cell tip, $\xi = \eta = 0$: $\frac{\partial\eta_B}{\partial\xi}(0) = \eta_B(0) = 0$.

(5) At the bottom of the root, $\xi = \pm 1$, $\eta = \eta_b$: $\eta_B(\pm 1) = \eta_b$; $\frac{\partial\eta_B}{\partial\xi}(\pm 1) = 0$.

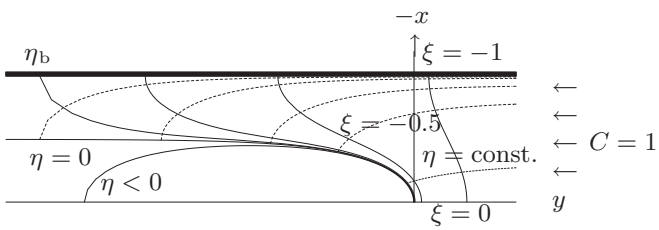

FIG. 3. The sketch of the orthogonal curvilinear coordinate system (ξ,η) based on the ST zero surface tension steady-state solutions.

IV. GENERALIZED ASYMPTOTIC SOLUTION IN THE OUTER REGION

We attempt to solve the system consisting of Eq. (3) and the boundary conditions (1)–(5) in the whole physical region $|\xi| \leqslant 1$, where $|\eta_B| \ll 1$. As a consequence, one may make the Taylor expansion for the interface conditions (4) and (5) around the interface $\eta = 0$ as follows:

$$\begin{aligned} &C_B(\xi,0) + \eta_B\frac{\partial C_B}{\partial\eta}(\xi,0) + \cdots \\ &\quad = y_* - \epsilon W\lambda_G[Y(\xi,0) + Y_\eta(\xi,0)\eta_B] \\ &\qquad - \frac{\epsilon^2\hat{\Gamma}}{\mathbb{M}W}\left[\mathcal{K}_0(\xi) - \frac{1}{\mathcal{G}_0}\frac{\mathrm{d}^2\eta_B}{\mathrm{d}\xi^2}\right] + o(\epsilon^2), \end{aligned} \quad (6)$$

where $\mathcal{K}_0(\xi) = \frac{\pi\lambda_0(1-\lambda_0)\cos(\frac{\pi\xi}{2})}{2[\lambda_0^2 + (1-2\lambda_0)\sin^2(\frac{\pi\xi}{2})]^{\frac{3}{2}}}$, and

$$\begin{aligned} &\frac{\partial C_B}{\partial\eta}(\xi,0) + \eta_B\frac{\partial^2 C_B}{\partial\eta^2}(\xi,0) - \frac{\partial\eta_B}{\partial\xi}\frac{\partial C_B}{\partial\xi}(\xi,0) \\ &\quad -\epsilon W(1-\kappa)\left[C_B(\xi,0) + \eta_B\frac{\partial C_B}{\partial\eta}(\xi,0)\right] \\ &\quad \times\left[Y_\xi(\xi,0)\frac{\partial\eta_B}{\partial\xi} - Y_\eta(\xi,0) - Y_{\eta\eta}(\xi,0)\eta_B\right] + O(\text{h.o.t}) = 0. \end{aligned} \quad (7)$$

Here it should be remarked that the system has a singularity at $\xi = \pm 1, \eta = 0$; as a consequence, the above approximate boundary conditions are applicable only in the outer region way from $\xi = \pm 1$.

Equation (3) plus the upstream far-field conditions, side-wall condition, tip smoothness conditions, and interface conditions (6)–(7) all together give an inhomogeneous system in the outer region. The general solution of an inhomogeneous system may include the following two parts:

$$\begin{aligned} C_{\mathrm{B}}(\xi,\eta,\epsilon) &= (\mathrm{I}) + (\mathrm{II}) = \bar{C}_{\mathrm{B}}(\xi,\eta,\varepsilon) + \tilde{C}_{\mathrm{B}}(\xi,\eta,\varepsilon), \\ \eta_{\mathrm{B}}(\xi,\epsilon) &= (\mathrm{I}) + (\mathrm{II}) = \bar{\eta}_{\mathrm{B}}(\xi,\epsilon) + \tilde{\eta}_{\mathrm{B}}(\xi,\epsilon). \end{aligned} \tag{8}$$

Part I of the solution, $\bar{C}_{\mathrm{B}}(\xi,\eta,\epsilon)$, is the particular solution of the inhomogeneous system, which may be expanded in the regular perturbation expansion (RPE) form; part II of the solution, $\tilde{C}_{\mathrm{B}}(\xi,\eta,\epsilon)$, is the general solution of the associated homogeneous system, which may be expanded in the singular perturbation (SPE) form. In next section, we attempt to find part I of the solution first.

A. Regular perturbation expansion of the solutions in the outer region

We introduce the slow far-field variable, $\tilde{\eta} = \epsilon\eta$, consider the concentration field as the functions of multiple variables $(\xi,\eta,\tilde{\eta})$, and solve it with the multiple-variables expansion method. We set $\bar{C}_{\mathrm{B}}(\xi,\eta,\epsilon) = \mathbb{C}(\xi,\eta,\tilde{\eta},\epsilon)$. The converted system with multiple variables is derived as

$$\begin{aligned} &\epsilon^2 \frac{\partial^2 \mathbb{C}}{\partial \tilde{\eta}^2} + \epsilon^2 W X_\xi \frac{\partial \mathbb{C}}{\partial \tilde{\eta}} + \frac{\partial^2 \mathbb{C}}{\partial \xi^2} + \frac{\partial^2 \mathbb{C}}{\partial \eta^2} + 2\epsilon \frac{\partial^2 \mathbb{C}}{\partial \eta \partial \tilde{\eta}} \\ &\quad + \epsilon W \left(Y_\xi \frac{\partial \mathbb{C}}{\partial \xi} + X_\xi \frac{\partial \mathbb{C}}{\partial \eta} \right) = 0 \end{aligned} \tag{9}$$

with the following boundary conditions:

(1) As $\eta \to \infty$,

$$\mathbb{C} \sim 1 + Q_0(\epsilon) e^{-W\tilde{\eta}}. \tag{10}$$

(2) Symmetric condition: at the side walls $\xi = \pm 1$,

$$\frac{\partial \mathbb{C}}{\partial \xi} = 0. \tag{11}$$

(3) Interface conditions: at $\eta = \tilde{\eta} = 0$,

$$\begin{aligned} &\mathbb{C}(\xi,0,0) + \eta_{\mathrm{B}} \frac{\partial \mathbb{C}}{\partial \eta}(\xi,0,0) + \epsilon \eta_{\mathrm{B}} \frac{\partial \mathbb{C}}{\partial \tilde{\eta}}(\xi,0,0) + \cdots \\ &\quad = y_* - \epsilon W \lambda_{\mathrm{G}} [Y(\xi,0) + Y_\eta(\xi,0)\eta_{\mathrm{B}}] \\ &\qquad - \frac{\epsilon^2 \hat{\Gamma}}{\mathbb{M} W} \left[\mathcal{K}_0(\xi) - \frac{1}{\mathcal{G}_0} \frac{\mathrm{d}^2 \eta_{\mathrm{B}}}{\mathrm{d}\xi^2} \right] + o(\epsilon^2), \end{aligned} \tag{12}$$

$$\begin{aligned} &\left(\frac{\partial \mathbb{C}}{\partial \eta} + \eta_{\mathrm{B}} \frac{\partial^2 \mathbb{C}}{\partial \eta^2} + \epsilon \eta_{\mathrm{B}} \frac{\partial^2 \mathbb{C}}{\partial \eta \partial \tilde{\eta}} - \frac{\partial \eta_B}{\partial \xi} \frac{\partial \mathbb{C}}{\partial \xi} \right) + \left(\epsilon \frac{\partial \mathbb{C}}{\partial \tilde{\eta}} + \epsilon \eta_{\mathrm{B}} \frac{\partial^2 \mathbb{C}}{\partial \tilde{\eta} \partial \eta} \right. \\ &\quad \left. + \epsilon^2 \eta_{\mathrm{B}} \frac{\partial^2 \mathbb{C}}{\partial \tilde{\eta}^2} \right) - \epsilon W (1-\kappa) \left(\mathbb{C} + \eta_{\mathrm{B}} \frac{\partial \mathbb{C}}{\partial \eta} + \epsilon \eta_{\mathrm{B}} \frac{\partial \mathbb{C}}{\partial \tilde{\eta}} \right) \\ &\quad \times \left[Y_\xi(\xi,0) \frac{\partial \eta_B}{\partial \xi} - Y_\eta(\xi,0) - Y_{\eta\eta}(\xi,0)\eta_{\mathrm{B}} \right] + O(\mathrm{h.o.t}) = 0. \end{aligned} \tag{13}$$

The solution of the above system may be expanded in the following RPE form:

$$\begin{aligned} \mathbb{C}(\xi,\eta,\tilde{\eta},\epsilon) &= \mathbb{C}_0(\xi,\eta,\tilde{\eta}) + \epsilon \mathbb{C}_1(\xi,\eta,\tilde{\eta}) + \cdots, \\ \eta_{\mathrm{B}}(\xi,\epsilon) &= \epsilon [h_1(\xi) + \epsilon h_2(\xi) + \cdots]. \end{aligned} \tag{14}$$

By substituting (14) into (9)–(13), one may successively derive each order approximate solutions.

B. Zeroth-order approximation $O(\epsilon^0)$

We have the solution

$$\mathbb{C}_0(\xi,\eta,\tilde{\eta}) = B_0(\tilde{\eta}), \tag{15}$$

where $B_0(\tilde{\eta})$ is subject to the interface condition $B_0(0) = y_{*0}$ and the far-field condition:

$$B_0(\tilde{\eta}) \sim 1 + \hat{Q}_0 e^{-W\tilde{\eta}}, \quad (\tilde{\eta} \to \infty). \tag{16}$$

C. First-order approximation $O(\epsilon^1)$

We derive the solution

$$\mathbb{C}_1(\xi,\eta,\tilde{\eta}) = -W\lambda_G Y(\xi,\eta) + B_1(\tilde{\eta}) + D_1(\tilde{\eta})\eta. \tag{17}$$

Noting that as $\eta \to \infty$, $Y(\xi,\eta) \sim \eta + \beta_0$, where $\beta_0 = -\frac{2(1-\lambda_0)}{\pi} \ln 2$, it is obtained that

$$\mathbb{C}_1(\xi,\eta,\tilde{\eta}) \sim B_1(\tilde{\eta}) - W\lambda_{\mathrm{G}}\beta_0 + [D_1(\tilde{\eta}) - W\lambda_{\mathrm{G}}]\eta, \ (\eta \to \infty).$$

To ensure the uniformly validity of the multiple variables expansion (MVE) solution in the limit $\eta \to \infty$, one must eliminate the secular term $[D_1(\tilde{\eta}) - W\lambda_{\mathrm{G}}]\eta$ on the right-hand side of the above expression by setting

$$D_1(\tilde{\eta}) = W\lambda_{\mathrm{G}}. \tag{18}$$

Furthermore, from the interface conditions we derive that

$$\begin{aligned} B_1(0) = y_{*1}, \quad B_1(\infty) = W\lambda_{\mathrm{G}}\beta_0, \\ W\lambda_G = -B_0'(0) - W\Delta_0, \end{aligned} \tag{19}$$

where we denote

$$\Delta_0 = \lambda_0[(1-\kappa)y_{*0} - \lambda_{\mathrm{G}}]. \tag{20}$$

The exact form of function $B_1(\tilde{\eta})$ remains to be determined.

D. The second-order approximation $O(\epsilon^2)$

We have the equation

$$\frac{\partial^2 \mathbb{C}_2}{\partial \xi^2} + \frac{\partial^2 \mathbb{C}_2}{\partial \eta^2} = \tilde{H}_2, \tag{21}$$

where

$$\begin{aligned} \tilde{H}_2 = &-2\frac{\mathrm{d}D_1}{\mathrm{d}\tilde{\eta}} + W^2\lambda_G \mathcal{G}^2(\xi,\eta) - W D_1(\tilde{\eta}) X_\xi(\xi,\eta) \\ &- \left[\frac{\mathrm{d}^2 B_0}{\mathrm{d}\tilde{\eta}^2} + W X_\xi(\xi,\eta) \frac{\mathrm{d}B_0}{\mathrm{d}\tilde{\eta}} \right], \end{aligned}$$

with the far-field condition, $\mathbb{C}_2 \sim \text{const.} \times e^{-W\tilde{\eta}}$, as $\eta \to \infty$; the side-wall condition, $\frac{\partial \mathbb{C}_2}{\partial \xi} = 0$ at $\xi = \pm 1$; and the interface conditions, at $\eta = 0, \tilde{\eta} = 0$:

$$\mathbb{C}_2 = y_{*2} - \left(\frac{\partial \mathbb{C}_1}{\partial \eta} + \frac{\partial \mathbb{C}_0}{\partial \tilde{\eta}} \right) h_1 - W\lambda_{\mathrm{G}} Y_{\eta,0}(\xi) h_1 - \frac{\hat{\Gamma}}{\mathbb{M} W} \mathcal{K}_0(\xi), \tag{22}$$

$$\frac{\partial \mathbb{C}_2}{\partial \eta} + B_1'(0) - W\frac{\Delta_0}{\lambda_0}(Y_{\xi,0}(\xi)h_1)' + W(1-\kappa)\mathbb{C}_1\lambda_0 = 0. \tag{23}$$

To eliminate the secular terms in the solution and ensure the uniform validity of the MVE solution, in the limit $\eta \to \infty$, it is necessary for the solution to satisfy the condition

$$\mathbb{H}_2(\tilde{\eta}) = \lim_{\eta\to\infty}\int_{-1}^{+1} \tilde{H}_2(\xi_1,\eta,\tilde{\eta})\mathrm{d}\xi_1 = 0, \tag{24}$$

which leads to

$$\left(\frac{\mathrm{d}^2 B_0}{\mathrm{d}\tilde{\eta}^2} + W\frac{\mathrm{d}B_0}{\mathrm{d}\tilde{\eta}}\right) = 0, \tag{25}$$

and consequently yields

$$\mathbb{C}_0 = B_0(\tilde{\eta}) = 1 + (y_{*0} - 1)e^{-W\tilde{\eta}}. \tag{26}$$

Furthermore, one may solve the solution $\mathbb{C}_2$ and h_1 in terms of the Fourier series expansion method. To this end, one can verify that the inhomogeneous Eq. (21) has the particular solution:

$$P_2(\xi,\eta,\tilde{\eta}) = -\tfrac{1}{2}[2D_1'(\tilde{\eta}) + B_0''(\tilde{\eta})]\eta^2 - \tfrac{1}{2}W[D_1(\tilde{\eta}) + B_0'(\tilde{\eta})] \times \eta Y(\xi,\eta) + \tfrac{1}{2}W^2\lambda_G Y^2(\xi,\eta). \tag{27}$$

At the tip $\xi = \eta = 0$, we have $P_2(0,0,0) = \frac{\partial}{\partial\eta}P_2(0,0,0) = 0$, while as $\eta \to \infty$,

$$P_2(\xi,\eta,\tilde{\eta}) \sim \tfrac{1}{2}\beta_0 W[W\lambda_G - B_0'(\tilde{\eta})]\eta + \tfrac{1}{2}W^2\lambda_G\beta_0^2.$$

We express the solution $\mathbb{C}_2(\xi,\eta,\tilde{\eta})$ in the form

$$\mathbb{C}_2(\xi,\eta,\tilde{\eta}) = B_2(\tilde{\eta}) + D_2(\tilde{\eta})\eta + P_2(\xi,\eta,\tilde{\eta}) + \phi_2(\xi,\eta,\tilde{\eta}), \tag{28}$$

where $\phi_2(\xi,\eta,\tilde{\eta})$ satisfies the Laplace equation. In order for the solution $\mathbb{C}_2(\xi,\eta,\tilde{\eta})$ to satisfy the far-field condition in the limit $\eta \to \infty$, one must set

$$D_2(\tilde{\eta}) = -\tfrac{1}{2}\beta_0 W[W\lambda_G - B_0'(\tilde{\eta})], \qquad B_2(\tilde{\eta}) = -\tfrac{1}{2}W^2\lambda_G\beta_0^2, \tag{29}$$

and assume that $\phi_2(\xi,\eta,\tilde{\eta}) \sim$ const. $\times\, \mathrm{e}^{-\mathrm{W}\tilde{\eta}}$, as $\eta \to \infty$.

By applying the interface conditions (22) and (23) to solution (28), it follows that, at $\eta = \tilde{\eta} = 0$,

$$-\tfrac{1}{2}W^2\lambda_G\beta_0^2 + \phi_2(\xi,0,0) + P_2(\xi,0,0) = y_{*2} + W\Delta_0 h_1(\xi,0,0) - \frac{\hat{\Gamma}}{\mathbb{M}W}\mathcal{K}_0(\xi), \tag{30}$$

and

$$\frac{\partial\phi_2}{\partial\eta}(\xi,0,0) + \frac{\partial P_2}{\partial\eta}(\xi,0,0) + D_2(0) + B_1'(0) + W(1-\kappa)\mathbb{C}_1(\xi,0,0)\lambda_0 = W\frac{\Delta_0}{\lambda_0}[Y_{\xi,0}(\xi)h_1]'. \tag{31}$$

To solve the above problem, we expand the functions $P_2(\xi,\eta,\tilde{\eta})$, $\phi_2(\xi,\eta,\tilde{\eta})$, and $h_1(\xi)$ in the following Fourier cosine series over the interval $(0 < \xi < 1)$:

$$\begin{cases} \phi_2(\xi,\eta,\tilde{\eta}) = \sum_{m=0}^{\infty} A_{2,m}(\tilde{\eta})\cos(m\pi\xi)e^{-m\pi\eta}, \\ P_2(\xi,\eta,\tilde{\eta}) = \sum_{m=0}^{\infty} E_{2,m}(\eta,\tilde{\eta})\cos(m\pi\xi); \\ h_1(\xi) = \sum_{m=0}^{\infty} B_{1,m}\cos(m\pi\xi), \end{cases} \tag{32}$$

in which we require that $A_{2,0}(\tilde{\eta}) = A_{2,0}(0)e^{-W\tilde{\eta}}$. Furthermore let $[Y_{\xi,0}(\xi)h_1(\xi)]' = \sum_{m=0}^{\infty}\mathbb{N}_m\cos(m\pi\xi)$. It is derived that

$$\mathbb{N}_m 2m\pi\int_0^1\sum_{n=0}^{\infty}[B_{1,n}\cos(n\pi\xi)]Y_{\xi,0}(\xi)\sin(m\pi\xi)\mathrm{d}\xi = 2m\pi\sum_{n=0}^{\infty}\mathcal{Q}_{m,n}B_{1,n}, \tag{33}$$

where $\mathcal{Q}_{m,n} = 2\int_0^1 Y_{\xi,0}(\xi)\cos(n\pi\xi)\sin(m\pi\xi)\mathrm{d}\xi$, $(m = 1, 2, \ldots; n = 0, 1, 2, \ldots)$. We find that $\mathcal{Q}_{m,n}$ may be written in the form, $\mathcal{Q}_{m,n} = -(1-\lambda_0)\widehat{\mathcal{Q}}_{m,n}$, where $\widehat{\mathcal{Q}}_{m,n}$ is the lower triangular matrix [see formula (2.539) in Ref. [29]]:

$$\widehat{\mathcal{Q}}_{m,n} = \begin{cases} 0 & (n > m) \\ (-1)^{m+n+1}2 & (n < m) \\ -1 & (n = m). \end{cases} \tag{34}$$

Moreover, let

$$\mathcal{K}_0(\xi) = \sum_{m=0}^{\infty}\alpha_m\cos(m\pi\xi), \qquad Y_0(\xi) = \sum_{m=0}^{\infty}\beta_m\cos(m\pi\xi), \tag{35}$$

where one may find that $\alpha_0 = 1/\lambda_0$, $\beta_0 = -(2\ln 2)(1-\lambda_0)/\pi$, $\beta_m = 2(-1)^{m-1}(1-\lambda_0)/(m\pi)$, $(m = 1, 2, \ldots)$. By substituting the above Fourier expansions into the interface conditions (30)–(31), one may derive that $B_{1,0} = 0$ and

$$\frac{\partial E_{2,0}}{\partial\eta}(0,0) + D_2(0) + B_1'(0) = -W(1-\kappa)\lambda_0(y_{*1} - W\lambda_G\beta_0), \qquad A_{2,0}(0) = \frac{1}{2}W^2\lambda_G\beta_0^2 + y_{*2} - \frac{\hat{\Gamma}}{\mathbb{M}W}\alpha_0 - E_{2,0}(0,0), \tag{36}$$

where

$$E_{2,0}(0,0) = \left[\frac{1}{6} + \frac{2(\ln 2)^2}{\pi^2}\right]W^2\lambda_G(1-\lambda_0)^2, \qquad \frac{\partial E_{2,0}}{\partial\eta}(0,0) = \frac{1}{2}\beta_0\lambda_0 W^2[(1-\kappa)y_{*0} + \lambda_G].$$

One can solve the two sets of constants $\{A_{2,n}(0), B_{1,n}\}(n = 1,2,\ldots)$. The interface shape function $h_1(\xi)$ is then fully determined. The values of $h_1(0)$ at the tip can be calculated numerically as $h_1(0) = \sum_{m=1}^{\infty}B_{1,m}$.

The numerical computations for the solutions $h_1(\xi)$ have been conducted for various cases. In Fig. 4(a), we show the variations of the interface shape function $\eta = h_1(\xi)$ for the typical case: $\lambda_0 = 0.6$. By fitting the numerical data in the vicinity of $\xi = -1$ on the log-log graphs, it is obtained that as $\xi \to -1$, $h_1(\xi) \sim \mathbb{a}_0(1+\xi)^{\alpha}(0 < \alpha < 1)$, as shown in Fig. 4(b). It yields that $h_1'(-1) = \infty$.

To plot the interface shape in the physical plane (X,Y), we apply the transformation (2) to calculate $X(\xi,\eta_s), Y(\xi,\eta_s)$. Therefore, approaching to he root as $\xi + 1 = \delta \to 0$ and

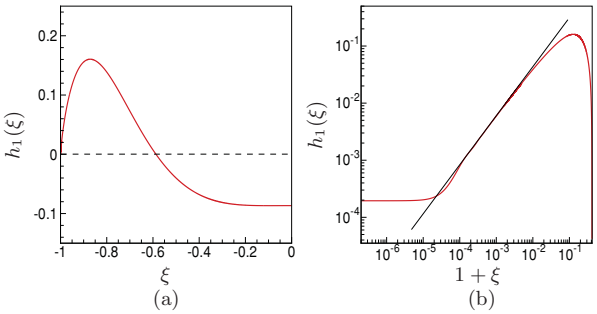

FIG. 4. (Color online) The characteristics solution $h_1(\xi)$ for the case $\epsilon = 0.1, \mathbb{M} = 6.0$, $\hat{\Gamma} = 0.3, \kappa = 0.1$, and $\lambda_G = 2.0, \lambda_0 = 0.6$. (a) The graph of the function $h_1(\xi)$ in the outer region; (b) the behavior of the function $h_1(\xi)$ near $\xi = -1$. The black line is $h_1 = 2.63(1+\xi)^{0.88}$. Due to the unavoidable existence of numerical truncation error in the computation, the graph of the solution $h_1(\xi)$ shown in the figure does not vanish as $\xi \to -1$ as it should, theoretically speaking.

$\eta_s \to 0$, we have $Y(\xi,\eta_s) \to -\infty$, and the width of the finger approaches to the following constant:

$$X(\xi,\eta_s) = \xi - \frac{2(1-\lambda_0)}{\pi}\tan^{-1}\left[\frac{\sin(\pi\xi)}{\cos(\pi\xi)+e^{\pi\eta_s}}\right] \approx -1 + \frac{2(1-\lambda_0)}{\pi}\tan^{-1}\left(\frac{\delta}{\eta_s}\right) \approx -1 + \frac{2(1-\lambda_0)}{\pi}\tan^{-1}\left[\frac{1}{\eta_s'(-1)}\right].$$

Thus, it is concluded that the root of finger always extends to infinity with $Y(\xi,\eta_s) \to -\infty$, $X(\xi,\eta_s) \to -1$.

E. The third-order approximation $O(\epsilon^3)$

Similar to what have been done for the system of second-order approximation, to eliminate the secular terms in the limit $\eta \to \infty$, one must apply the necessary condition to the inhomogeneous term $\tilde{H}_3(\xi,\eta,\tilde{\eta})$:

$$\mathbb{H}_3(\tilde{\eta}) = \lim_{\eta\to\infty}\int_{-1}^{+1}\tilde{H}_3(\xi_1,\eta,\tilde{\eta})\,d\xi_1 = 0. \tag{37}$$

By using the far-field conditions of the first-order approximation, it is then derived that $B_1(\tilde{\eta}) = y_{*1}e^{-W\tilde{\eta}} + W\lambda_G\beta_0(1-e^{-W\tilde{\eta}})$, and we eventually obtain $\mathbb{C}_1 = W\lambda_G\eta - W\lambda_G Y(\xi,\eta) + [W\lambda_G\beta_0 + (y_{*1} - W\lambda_G\beta_0)e^{-W\tilde{\eta}}]$, where the constant y_{*1} can be derived from (36) as follows:

$$y_{*1} = \frac{\beta_0 W}{2[(1-\kappa)\lambda_0 - 1]}\left\{(y_{*0} - 1 - \lambda_G) + \lambda_0\lambda_G \times\left[(1-\kappa)\left(2 - \frac{1}{\lambda_G}y_{*0}\right) - 1\right]\right\}. \tag{38}$$

Moreover, we obtain

$$\lambda_0 = \frac{y_{*0} - 1 - \lambda_G}{(1-\kappa)y_{*0} - \lambda_G}. \tag{39}$$

For the special isothermal case $\lambda_G = 0$, the above formula reduces to that obtained by Pelcé and Pumir [4].

We do not attempt to proceed any further for higher-order approximate solutions. Here we point out only that the RPE solution obtained possesses the following characteristics.

(1) It is a uniquely determined particular solution in the outer region without any arbitrary constant.

(2) Its mass balance condition at the interface, in any kth-order approximation, always contains the following two terms:

$$\frac{\partial\mathbb{C}_k}{\partial\eta} - W\frac{\Delta_0}{\lambda_0}[Y_\xi(\xi,0)h_k]' + \cdots = 0.$$

Since the function $Y_\xi(\xi,0)$ has the simple pole singularity at $\xi = \pm 1$, to guarantee the regularity of concentration function $\mathbb{C}_k(\xi,\eta)$ at the points $\xi = \pm 1, \eta = 0$, we must have the solution $h_k(\pm 1) = 0$. Therefore, it is deduced that the interface shape given by the Nth-order (RPE) approximate solution, $\eta = \bar{\eta}_B(\xi,\epsilon) = \sum_{n=0}^{N}\epsilon^{n+1}h_n(\xi)$, will always not have a closure at $\xi = \pm 1$, no matter how many terms are included.

(3) The value of the above (RPE) solution at the tip does not vanish, namely, $h_1(0) \neq 0$, which is inconsistent with the tip condition $\eta_B(0) = 0$. Therefore, the RPE solution obtained is not valid in the region near the cell tip. In other words, it cannot be considered as the outer solution yet.

To obtain the outer solution, one must include the general solution of the associated homogeneous system, $\{\tilde{C}_B(\xi,\eta,\varepsilon); \tilde{\eta}_B(\xi,\epsilon)\}$.

F. Singular perturbation expansion part of the solution in the outer region

The general solution of the associated homogeneous system may have multiple length scales and can be expanded in the SPE form with multiple variables: $\{\xi,\eta,\xi_+,\eta_+\}$, defined as $\xi_+ = 1/\sqrt{\epsilon\hat{\Gamma}}\int_0^\xi k(\xi_1,\eta)d\xi_1$; $\eta_+ = 1/\sqrt{\epsilon\hat{\Gamma}}\int_0^\eta k(\xi,\eta_1)d\eta_1$, where $k(\xi,\eta) = k_0(\xi,\eta) + \epsilon k_1(\xi,\eta) + \cdots$ [30,31].

The system for the leading-order approximation, $\tilde{C}_B(\xi,\eta,\varepsilon) \approx \tilde{\mathbb{C}}_0(\xi,\eta,\xi_+,\eta_+)$, and $\tilde{\eta}_B(\xi,\epsilon) \approx \tilde{h}_0(\xi,\xi_+)$ is derived as

$$\frac{\partial^2\tilde{\mathbb{C}}_0}{\partial\xi_+^2} + \frac{\partial^2\tilde{\mathbb{C}}_0}{\partial\eta_+^2} = 0, \tag{40}$$

with the following boundary conditions:

(1) At the side wall, $\xi = 1$

$$\frac{\partial\tilde{\mathbb{C}}_0}{\partial\xi_+} = 0. \tag{41}$$

(2) On the interface $\eta = \eta_+ = 0$: Let $k_0(\xi,0) = \bar{k}_0(\xi)$, we have

$$\tilde{\mathbb{C}}_0 = W\Delta_0\tilde{h}_0 + \frac{\bar{k}_0^2}{\mathbb{M}W\mathcal{G}_0(\xi,0)}\frac{\partial^2\tilde{h}_0}{\partial\xi_+^2}, \tag{42}$$

$$\bar{k}_0\frac{\partial\tilde{\mathbb{C}}_0}{\partial\eta_+} + WY_{\xi,0}(\xi,0)\bar{k}_0[\lambda_G - (1-\kappa)y_{*0}]\frac{\partial\tilde{h}_0}{\partial\xi_+} = 0. \tag{43}$$

(3) At the tip, $\xi = \xi_+ = 0$,

$$\frac{\partial\tilde{h}_0}{\partial\xi_+} = 0. \tag{44}$$

We consider the mode solutions for the above system:

$$\tilde{\mathbb{C}}_0 = \tilde{A}_0(\xi,\eta)\exp(i\xi_+ - \eta_+), \tilde{h}_0 = \bar{D}_0\exp(i\xi_+), \tag{45}$$

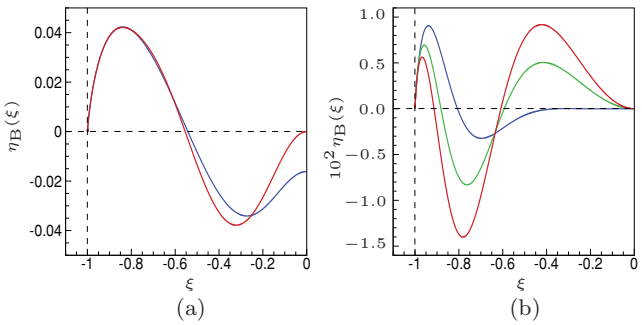

FIG. 5. (Color online) (a) The graph of the outer solution for the case $\epsilon = 0.1$, $\kappa = 0.1$, $\lambda_G = 0.8$, $\lambda_0 = 0.4$, $\mathbb{M} = 1.0$, $\hat{\Gamma} = 2$. The top on the left is the graph of the outer solution $\eta_B(\xi)$(with inclusion of the SPE part) over $(-1 < \xi \leqslant 0)$; the bottom on the right is the graph of the RPE part of outer solution $\epsilon h_1(\xi)$. (b) The graphs of the full solutions $\eta_B(\xi)$ in the (ξ,η) plane for the typical cases: $\epsilon = 0.1$, $\kappa = 0.1$,$\lambda_G = 2.0$, $\lambda_0 = 0.6$, $\mathbb{M} = 1.0$, and $\hat{\Gamma} = 1.0$, 1.5, 2.0 from bottom to top on the right-hand side of the figure.

where the coefficient $\bar{D}_0$ is a constant. With the notation $\tilde{A}_0(\xi,0) = \bar{A}_0(\xi)$, it is derived from the interface conditions (42) and (43) that

$$\bar{A}_0(\xi) = \bar{D}_0\left[W\Delta_0 - \frac{\bar{k}_0^2}{\mathbb{M}W\mathcal{G}_0(\xi,0)}\right],$$

and

$$\bar{k}_0^3 = \bar{k}_0\mathbb{M}W^2\Delta_0\mathcal{G}_0(\xi,0)\left[1 + \frac{\mathrm{i}}{\lambda_0}Y_{\xi,0}(\xi,0)\right].$$

There are three roots for $\bar{k}_0$:

$$\bar{k}_0^{(1)}(\xi) = \bar{k}_s(\xi), \quad \bar{k}_0^{(2)}(\xi) = -\bar{k}_s(\xi), \quad \bar{k}_0^{(3)}(\xi) = 0, \quad (46)$$

where $\bar{k}_s(\xi) = W\sqrt{\mathbb{M}\Delta_0\mathcal{G}_0(\xi,0)}[1 + \frac{\mathrm{i}}{\lambda_0}Y_{\xi,0}(\xi,0)]^{\frac{1}{2}}$, $(-1 < \xi \leqslant 0)$. Here we have chosen that $\mathrm{Re}[\bar{k}_s(\xi)] > 0$. In accordance with the above, we obtain three fundamental solutions:

$$H_1(\xi) = e^{\frac{\mathrm{i}}{\sqrt{\epsilon\hat{\Gamma}}}\chi(\xi)}, H_2(\xi) = e^{-\frac{\mathrm{i}}{\sqrt{\epsilon\hat{\Gamma}}}\chi(\xi)}, H_3(\xi) = 1, \quad (47)$$

where we have defined

$$\chi(\xi) = \int_0^\xi \bar{k}_s(\xi_1)\,d\xi_1 = \chi_R(\xi) + \mathrm{i}\chi_I(\xi). \quad (48)$$

Note that $\mathrm{Im}\{\bar{k}_s(\xi)\} > 0$, $(-1 < \xi \leqslant 0)$. The solution $H_1(\xi)$ should be ruled out, because away from the interface, as η increases, the corresponding concentration field tends to infinity exponentially, violating the far-field condition. As a consequence, the physically acceptable solution is a linear combination of two fundamental solutions $\{H_2(\xi), H_3(\xi)\}$. Note also that as $\xi \to -1$, we have

$$\mathcal{G}_0(\xi,0) \sim -(1-\lambda_0)\tan\left(\frac{\pi\xi}{2}\right),$$

$$Y_{\xi,0}(\xi,0) = -(1-\lambda_0)\tan\left(\frac{\pi\xi}{2}\right), \quad (49)$$

$$\bar{k}_s(\xi) \sim -\frac{1}{\sqrt{2}}(1+\mathrm{i})W(1-\lambda_0)\sqrt{\frac{\mathbb{M}\Delta_0}{\lambda_0}}\tan\left(\frac{\pi\xi}{2}\right).$$

Consequently $\mathrm{Re}[\bar{k}_s(\xi)] \to +\infty$, $\mathrm{Im}[\bar{k}_s(\xi)] \to +\infty$, as $\xi \to -1$. This implies that as $\xi \to -1$, the solution $|H_2(\xi)| \to 0$ exponentially, which is subdominant compared with the solution $H_3(\xi) = 1$.

In terms of the tip condition $\eta_B(0,\epsilon) = 0$, one may finally derive the outer solution for the interface shape as

$$\eta_B(\xi,\epsilon) = \epsilon\left\{h_1(\xi) - h_1(0)e^{\frac{\chi_I(\xi)}{\sqrt{\epsilon\hat{\Gamma}}}}\cos\left[\frac{\chi_R(\xi)}{\sqrt{\epsilon\hat{\Gamma}}}\right]\right\} + \cdots. \quad (50)$$

The graph of the outer solution for interface shape function $\eta_B(\xi)$ and the corresponding RPE part of the solution is shown in Fig. 5(a) for some typical case, whereas the variation of the interface shape function of the outer solution with the parameter $\hat{\Gamma}$ is shown in Fig. 5(b).

In Fig. 6, we show the interface shapes on (X,Y) plane for some typical cases (a)–(c) and compare the theoretical results with the experimental photos (a)–(c) given by Georgelin and Pocheau for the same cases with no adjustable parameter [20]. In Fig. 7, we show the comparison of interface shape between the theoretical result and the experimental data for the typical case: the pulling velocity $V = 12\,\mu$m/s, the temperature gradient $G_D = 140$ K/cm, and the primary spacing $\ell_w = 90\,\mu$m and the tip radius $\ell_t = 22.4\,\mu$m. It is seen that the

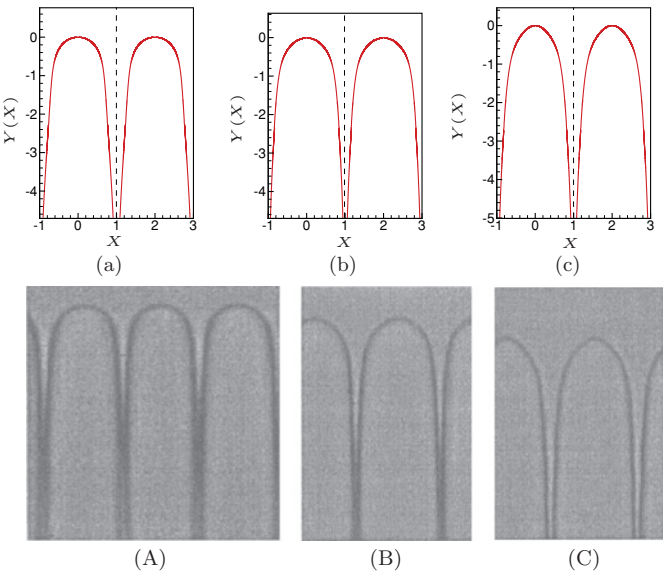

FIG. 6. (Color online) The interface shapes in (X,Y) plane described by the outer solutions for the typical cases experimentally observed by Georgelin and Pocheau [20], which yield the dimensionless parameters: $\kappa = 0.29$, $\mathbb{M} = 0.084\,32$, and (a) $\epsilon = 0.1289$, $W_0 = 1.725$; $\lambda_0 = 0.6020$, $\lambda_G = 0.7826$, $\hat{\Gamma} = 0.011\,64$, $\alpha = 0.88$, $\mathbb{a}_0 = 1.9054$; (b) $\epsilon = 0.1991$, $W_0 = 2.007$; $\lambda_0 = 0.5760$, $\lambda_G = 0.7826$, $\hat{\Gamma} = 0.003\,157$, $\alpha = 0.88$, $\mathbb{a}_0 = 2.2387$; (c) $\epsilon = 0.2667$, $W_0 = 3.000$; $\lambda_0 = 0.5077$, $\lambda_G = 0.3913$, $\hat{\Gamma} = 0.002\,629$, $\alpha = 0.88$, $\mathbb{a}_0 = 1.7782$. The photos (a)–(c) are the interface shapes observed in the experiments by Georgelin and Pocheau in the same cases corresponding to (a)–(c), respectively. The dimensional experimental data for these cases are (a) Pulling velocity: $V = 12.0\,\mu$m/s, primary spacing $2\ell_w = 50.0\,\mu$m, gradient of temperature $G_D = 140.0 \times 10^{-4}$ K/(μm), and tip radius $\ell_t = 14.5\,\mu$m; (b) Pulling velocity: $V = 12.0\,\mu$m/s, primary spacing $2\ell_w = 90.0\,\mu$m, gradient of temperature $G_D = 140.0 \times 10^{-4}$ K/(μm), and tip radius $\ell_t = 22.4\,\mu$m; (c) Pulling velocity: $V = 24.0\,\mu$m/s, primary spacing $2\ell_w = 90.0\,\mu$m, gradient of temperature $G_D = 140.0 \times 10^{-4}$ K/(μm), and tip radius $\ell_t = 15.0\,\mu$m.

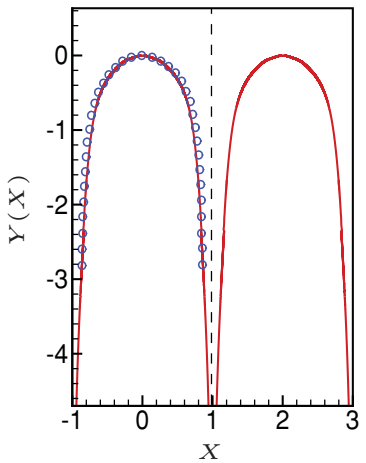

FIG. 7. (Color online) The interface shape in the (X,Y) plane for the typical case: $\kappa = 0.29$, $c_\infty = 1.2\,\text{mol}\%$, and the pulling velocity $V = 12\mu\text{m/s}$, the temperature gradient $G_\text{D} = 140.0 \times 10^{-4}\,\text{K}/(\mu\text{m})$, primary spacing $\ell_w = 90\,\mu\text{m}$, and the tip radius $\ell_\text{t} = 22.4\,\mu\text{m}$. In the figures, circles represent are experimental data obtained by Pocheau *et al.* [20].

theoretical results are in very good quantitative agreement with the experimental observation. Note that the theoretical model is 2D with no anisotropy of surface tension, while the experimental samples given by Georgelin and Pocheau are not perfectly 2D and have a small amount of anisotropy. The results show that the effects of three dimensionality and anisotropy of surface tension on the interface shapes in the region not close to the bottom of the root are insignificant at least in the cases under study, in spite that these physical properties may have a noticeable quantitative effects on the selection of cellular growth, as revealed by the most recent numerical simulations [17,18].

In terms of the above composite solution and the formulas $\bar{\ell}_\text{t} = 1 = \mathcal{K}\{\eta_\text{B}\}(0,\epsilon)/W$, one may finally derive that the primary spacing $W = W_0 + \epsilon W_1 + \cdots$, where

$$W_0 = \mathcal{K}_0(0) = \frac{\pi(1-\lambda_0)}{2\lambda_0^2},$$
$$W_1 = \mathcal{K}_1(0) = -\frac{1}{\lambda_0}\eta_\text{B}''(0). \tag{51}$$

The outer solution obtained may also yield the concentration of impurity along the interface in the outer region:

$$\mathbb{C} = y_{*0} + \epsilon\mathbb{C}_1(\xi,0,0) + \epsilon^2\mathbb{C}_2(\xi,0,0) - \epsilon^2 h_1(0)\left[W\Delta_0 - \frac{\bar{k}_0^2(\xi)}{\mathbb{M}W\mathcal{G}_0(\xi,0)}\right] \times e^{\frac{\chi_\text{I}(\xi)}{\sqrt{\epsilon\hat{\Gamma}}}}\cos\left(\frac{\chi_\text{R}(\xi)}{\sqrt{\epsilon\hat{\Gamma}}}\right) + \cdots \tag{52}$$

as well as the location of the cell tip in the experimental system via the solution:

$$y_* = y_{*0} + \epsilon y_{*1} + \cdots,$$

where

$$y_{*0} = \frac{1 + \lambda_\text{G}(1-\lambda_0)}{1 - \lambda_0(1-\kappa)},$$

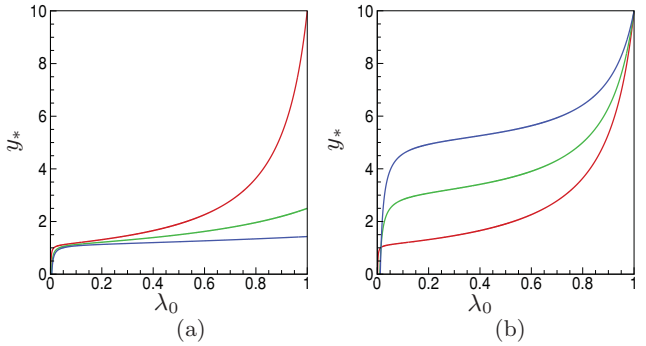

FIG. 8. (Color online) The variation of y_* with λ_0 for the cases $\epsilon = 0.1$ and (a) $\lambda_G = 0.1$, and $\kappa = 0.1, 0.4, 0.7$ from top to bottom; (b) $\kappa = 0.1$, and $\lambda_G = 0.1, 2.0, 4.0$ from bottom to top.

$$y_{*1} = \frac{\beta_0 W}{2[(1-\kappa)\lambda_0 - 1]}\left\{(y_{*0} - 1 - \lambda_\text{G}) + \lambda_0\lambda_\text{G} \times \left[(1-\kappa)\left(2 - \frac{1}{\lambda_\text{G}}y_{*0}\right) - 1\right]\right\}.$$

By neglecting the higher-order terms $O(\epsilon^2)$, one may approximately write the impurity concentration at the tip as $\mathbb{C}_\text{tip} \approx y_*$. The variation of y_* with λ_0 under different growth conditions and material properties are shown in Fig. 8(a)–8(b).

Moreover, the parameter y_* determines the tip undercooling temperature, as the function

$$T_\text{tip}(\lambda_\text{G},\epsilon) = T_\text{B}(0,0) = \epsilon G y_0 = \mathbb{M}y_* \approx \mathbb{M}(y_{*0} + \epsilon y_{*1}),$$

depending on the parameters $\lambda_0,\kappa,\lambda_\text{G}$, and ϵ.

Recall the constitutional instability criterion that given the gradient of temperature G, when $V = V_c$, $\lambda_\text{G} = \hat{\lambda}_\text{G} = \frac{(1-\kappa)}{\kappa}$, the flat interface becomes unstable. It is then deduced that as a necessary condition, $0 < \lambda_\text{G} < \hat{\lambda}_\text{G} = \frac{(1-\kappa)}{\kappa}$ must hold for the system of cellular growth. Recall that $\lambda_\text{G} = -\frac{\kappa_\text{D}}{mC_\infty}\frac{(G)_\text{D}}{V}$ and $\hat{\lambda}_\text{G} = -\frac{\kappa_\text{D}}{mC_\infty}\frac{(G)_\text{D}}{V_c}$, we may write $\lambda_\text{G} = \hat{\lambda}_\text{G}\frac{V_c}{V}$.

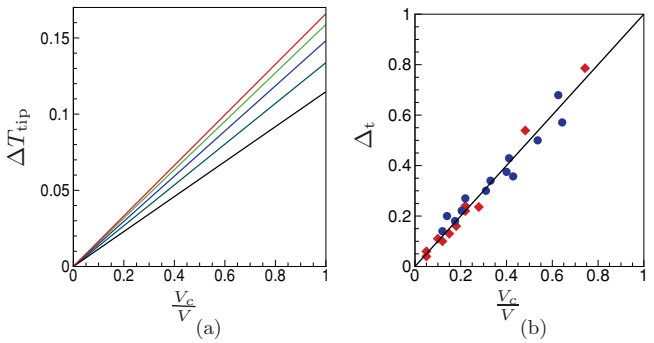

FIG. 9. (Color online) (a) The variation of ΔT_tip with λ_G for the cases $\epsilon = 0.1$, $\kappa = 0.3$, $\mathbb{M} = 0.084\,32$, and $\lambda_0 = 0.3, 0.4, 0.5, 0.6, 0.7$ (or $W_0 = 12.2173, 5.8905, 3.1415, 1.7453, 0.9617$) from top to bottom. (b) The universal scaling law for system of arrayed cellular growth. The experimental data are from Pocheau *et al.* for the directional solidification system of impure SCN [21]. The solid full squares are for the case $G_\text{D} = 78.0 \times 10^{-4}\,\text{K}/(\mu\text{m})$, and the full circles are for the case $G_\text{D} = 140.0 \times 10^{-4}\,\text{K}/(\mu\text{m})$.

Now let us take limit $V \to \infty$, or $\lambda_G \to 0$ with fixed C_∞ and temperature gradient $(G)_D$ and denote the limit as

$$\lim_{\lambda_G \to 0} T_{tip}(\lambda_G,\epsilon) = \frac{\mathbb{M}}{1-\lambda_0(1-\kappa)} = T_L(C_\infty).$$

Thus, the difference of temperature $\Delta T_{tip} = |T_{tip}(\lambda_G,\epsilon) - T_L(C_\infty)|$ can be derived as

$$\begin{aligned}\Delta T_{tip} &= |T_{tip}(\lambda_G,\epsilon) - T_L(C_\infty)| \\ &= \mathbb{M}\mathcal{A}\lambda_G = \mathbb{M}\hat{\mathcal{A}}V_c/V, \end{aligned} \tag{53}$$

where

$$\mathcal{A} = \frac{(1-\lambda_0)}{1-\lambda_0(1-\kappa)}\left[1 - \epsilon \ln 2\frac{\kappa(1-\lambda_0)}{\lambda_0}\right], \quad \hat{\mathcal{A}} = \hat{\lambda}_G\mathcal{A}$$

are the functions of the parameters $(\epsilon,\kappa,\mathbb{M})$ and λ_0 (or W_0). In Fig. 9(a), we show the variations of ΔT_{tip} with parameter V_c/V under different growth conditions and given material properties. It is seen that the graph of ΔT_{tip} is a set of straight lines passing through the origin with different slopes. Furthermore, we take the limit $V \to V_c$ or $\lambda_G \to \hat{\lambda}_G$ with fixed C_∞ and $(G)_D$ and denote

$$\lim_{\lambda_G \to \hat{\lambda}_G} T_{tip}(\lambda_G,\epsilon) = T_S(C_\infty).$$

Assume that the formula (53) can be approximately applied to the regime $V \approx V_c$ or $\lambda_G \approx \hat{\lambda}_G$. In terms of the formula (53), one derives

$$|T_S(C_\infty) - T_L(C_\infty)| = \hat{\lambda}_G\mathbb{M}\mathcal{A}.$$

Following the notations used by Pocheau *et al.* [21], we define the normalized tip temperature as $\Delta_t = |T_{tip}(\lambda_G,\epsilon) - T_L(C_\infty)|/|T_S(\infty) - T_L(C_\infty)|$ and the reduced pulling speed as $\nu = \frac{V}{V_c}$. Then we derive that

$$\Delta_t = \lambda_G/\hat{\lambda}_G = V_c/V = \frac{1}{\nu}, \quad \text{or} \quad \Delta_t\nu = 1, \tag{54}$$

which yields a straight line with the unit slope on the $(\Delta,1/\nu)$ plane and is a universal scaling law applicable for any arrayed-cellular growth system under any growth conditions.

It is known that under given control parameters $V,(G)_D,\mathbb{M}$, the primary spacing W_0 (or λ_0) varies in different experiments depending on the history of growth, so does the tip location parameter y_*. However, as indicated by Pocheau *et al.* [21]: "in practice, the variation of Δ_t with W_0 stands beyond our accuracy"; such a variation of primary spacing, practically, does not noticeably affect the value of Δ_t in the whole extent of W_0. Moreover, Pocheau *et al.* argued that the limit value of tip temperature $T_L(C_\infty)$ is very close to the liquidus, while the limit value $T_S(C_\infty)$ is close to the solidus temperature. Both temperatures are measurable with the flat interface.

Thus, the scaling law (54) can be examined by their experimental data. In Fig. 9(b) we show the comparison of the scaling law (54) with the experimental data under various growth conditions given by Pocheau *et al.* [21]. The best fitting line to the experimental data claimed by Pocheau *et al.* has the slope 0.998. It is seen that our theoretical result is in a very good agreement with their experimental observations.

The solution (50) obtained, however, is still not applicable in the region near the root. It fails to satisfy the root smoothness conditions: $\eta_B(-1,\epsilon) = \eta_T(-1,\epsilon) > 0$ and $\eta'_B(-1,\epsilon) = 0$, yielding the interface shape not closed at $\xi = \pm 1$. Hence, it provides no information on the location of the bottom of the root, the total length of the cells, and the concentration of impurity at the bottom of the root. In order to find the global solution of the cellular growth, we need to derive its inner solution in the root region.

V. GENERALIZED ASYMPTOTIC SOLUTION IN THE ROOT REGION

The root region can be specified as $|\xi + 1| \ll 1; |\eta - \eta_T(\xi)| \ll 1$. The central line of the root region is given by the function $\eta = \eta_T(\xi)$, which is assumed to be an approximation of the interface shape function in the root region. We introduce the root variables $\hat{\xi}$ and $\hat{\eta}$ as follows:

$$\hat{\xi} = \frac{1+\xi}{\delta(\epsilon)}, \quad \hat{\eta} = \frac{\eta - \eta_T(\xi)}{\delta(\epsilon)}. \tag{55}$$

From the asymptotic behavior of the outer solution $h_1(\xi) \sim \mathbb{a}_0(1+\xi)^\alpha$, as $(\xi \to -1)$, that was derived in the last section, we deduce that in the far field of the root region $\eta_B(\xi) \approx \epsilon\,\mathbb{a}_0(1+\xi)^\alpha$. To match the outer solution, we derive that in the far field of the root region, $\eta_T(\xi) = \delta(\epsilon)\hat{\eta}_T(\hat{\xi}) = \mathbb{a}_0\epsilon(1+\xi)^\alpha = \mathbb{a}_0\epsilon\delta^\alpha(\epsilon)\hat{\xi}^\alpha$. Thus, one must set $\delta(\epsilon) = \epsilon\delta^\alpha(\epsilon)$ or $\delta(\epsilon) = \epsilon^{\frac{1}{1-\alpha}}$, and write $\hat{\eta}_T(\hat{\xi}) = \mathbb{a}_0\hat{\xi}^\alpha$.

Near the bottom of the root $\hat{\xi} = 0$, the approximation $\eta_B(\xi) \approx \mathbb{a}_0\epsilon(1+\xi)^\alpha$ is no longer valid, as it violates the root smoothness condition $\hat{\eta}'_T(0) = 0$. Instead, one may write $\eta_B(\xi) = \delta(\epsilon)\hat{\eta}_T(\hat{\xi})$ and $\hat{\eta}_T(\hat{\xi}) = [\hat{\eta}_b + \mathbb{a}_2\hat{\xi}^2 + \mathbb{a}_3\hat{\xi}^3]$. Thus, to describe the interface shape function $\hat{\eta}_B(\hat{\xi})$, one needs to divide the root region into three subregions with an internal transition point $0 < \hat{\xi}_T < \infty$ and express the interface shape function $\hat{\eta}_T(\hat{\xi})$ with different forms in different subregions, such that

(1) In subregion (I): as $(\hat{\xi}_T < \hat{\xi} < \infty)$, $\hat{\eta}_T(\hat{\xi}) = \hat{\eta}_T^{(I)}(\hat{\xi}) = \mathbb{a}_0\hat{\xi}^\alpha + \cdots$.

(2) In subregion (II): as $(0 \leqslant \hat{\xi} < \hat{\xi}_T)$, $\hat{\eta}_T(\hat{\xi}) = \hat{\eta}_T^{(II)}(\hat{\xi}) = \delta(\epsilon)[\bar{\eta}_b + \bar{\mathbb{a}}_2\hat{\xi}^2 + \delta(\epsilon)\bar{\mathbb{a}}_3\hat{\xi}^3] + \cdots$.

(3) In subregion (III) centered at $\hat{\xi} = \hat{\xi}_T$ and between subregion (I) and (II): $\hat{\eta}_T(\hat{\xi})$ transits from $\hat{\eta}_T^{(I)}(\hat{\xi})$ to $\hat{\eta}_T^{(II)}(\hat{\xi})$.

To satisfy the matching conditions, we require that at $\hat{\xi} \to \hat{\xi}_T^\pm$, $\hat{\eta}_T^{(I)}(\hat{\xi}_T) = \hat{\eta}_T^{(II)}(\hat{\xi}_T)$ and $\frac{d^k}{d\hat{\xi}^k}\hat{\eta}_T^{(I)}(\hat{\xi}_T) = \frac{d^k}{d\hat{\xi}^k}\hat{\eta}_T^{(II)}(\hat{\xi}_T)$, $(k = 1,2,\ldots)$, where $\hat{\xi}_T$ may depend on the parameter ϵ and is expected to have the asymptotic expansion

$$\hat{\xi}_T(\epsilon) = \hat{\xi}_*(\epsilon)[1 + d_1\delta(\epsilon) + \cdots], \quad (\text{as} \quad \epsilon \to 0).$$

So, in the leading-order approximation, we may write

$$\hat{\eta}_T(\hat{\xi}) = \begin{cases} \mathbb{a}_0\hat{\xi}^\alpha, & (\text{I}) : (\hat{\xi}_* < \hat{\xi} < \infty), \\ \hat{\eta}_b + \mathbb{a}_2\hat{\xi}^2 + \mathbb{a}_3\hat{\xi}^3, & (\text{II}) : (0 \leqslant \hat{\xi} < \hat{\xi}_*). \end{cases} \tag{56}$$

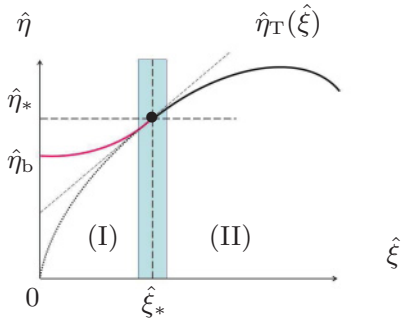

FIG. 10. (Color online) The sketch of the function $\hat{\eta}_{\mathrm{T}}$ in the root region.

The parameters $\hat{\eta}_*$, $\hat{\eta}_{\mathrm{b}}$, and $\mathbb{a}_2$ are the functions of $\hat{\xi}_*$ as given here:

$$\hat{\eta}_* = \mathbb{a}_0\hat{\xi}_*^{\alpha},\ \hat{\eta}_{\mathrm{b}} = \left[1 - \frac{\alpha(5-\alpha)}{6}\right]\hat{\eta}_*,\quad \mathbb{a}_2 = \frac{\alpha(3-\alpha)\hat{\eta}_*}{2\hat{\xi}_*^2},$$
$$\mathbb{a}_3 = -\frac{\alpha(2-\alpha)\hat{\eta}_*}{3\hat{\xi}_*^3},$$

and $\hat{\xi}_*$ is the eigenvalue to be determined. The graph of function $\hat{\eta}_{\mathrm{T}}(\hat{\xi})$ is sketched in Fig. 10. The above-defined central line function $\hat{\eta}_{\mathrm{T}}(\hat{\xi})$ is smooth with a continuous second-order derivative in the entire root region ($0 \leqslant \hat{\xi} < \infty$), but it has the discontinuity in the third-order derivative at $\hat{\xi} = \hat{\xi}_*$. As a consequence, the inner system has singularity at the point $\hat{\xi}_*$.

We express the interface shape function in the following form:

$$\eta_{\mathrm{B}}(\xi,\epsilon) = \delta(\epsilon)\big[\hat{\eta}_{\mathrm{T}}(\hat{\xi}) + \hat{\eta}_{\mathrm{B}}(\xi,\epsilon) + \cdots\big], \tag{57}$$

and further assume that in the root region the interface shape function $|\hat{\eta}_{\mathrm{B}}(\hat{\xi},\epsilon)| \ll 1$. Thus the interface condition may be linearized around the interface $\hat{\eta}_{\mathrm{T}}(\hat{\xi})$.

In the root region, the concentration field with inner variables $\{\hat{\xi},\hat{\eta}\}$ is expressed as $C = \hat{C}(\hat{\xi},\hat{\eta},\epsilon)$. Letting $\epsilon \to 0$ with fixed $\hat{\xi},\hat{\eta}$, we expand the coordinate functions in the following asymptotic forms, respectively [26–31]:

$$\begin{aligned}
\hat{Y}(\hat{\xi},\hat{\eta},\epsilon) &= Y[-1+\delta(\epsilon)\hat{\xi};\delta(\epsilon)(\hat{\eta}+\hat{\eta}_{\mathrm{T}})]\\
&\sim \ln\delta(\epsilon)\hat{Y}_* + \hat{Y}_0(\hat{\xi},\hat{\eta}) + \delta(\epsilon)\hat{Y}_1(\hat{\xi},\hat{\eta}) + \cdots,\\
Y_\eta(\xi,\eta) &= \frac{1}{\delta(\epsilon)}\hat{Y}_{\hat{\eta}}(\hat{\xi},\hat{\eta},\epsilon) \sim \frac{1}{\delta(\epsilon)}\hat{Y}_{\hat{\eta},0}(\hat{\xi},\hat{\eta})\\
&\quad + \hat{Y}_{\hat{\eta},1}(\hat{\xi},\hat{\eta}) + \cdots,\\
Y_\xi(\xi,\eta) &= \frac{1}{\delta(\epsilon)}\hat{Y}_{\hat{\xi}}(\hat{\xi},\hat{\eta},\epsilon) \sim \frac{1}{\delta(\epsilon)}\hat{Y}_{\hat{\xi},0}(\hat{\xi},\hat{\eta}) + \cdots,
\end{aligned} \tag{58}$$

where

$$\begin{aligned}
\hat{Y}_* &= \frac{2(1-\lambda_0)}{\pi},\quad \hat{Y}_0 = \frac{(1-\lambda_0)}{\pi}\ln\frac{\pi^2[(\hat{\eta}+\hat{\eta}_{\mathrm{T}})^2+\hat{\xi}^2]}{4},\\
\hat{Y}_1 &= \lambda_0(\hat{\eta}+\hat{\eta}_{\mathrm{T}}),\\
\hat{Y}_{\hat{\eta},0}(\hat{\xi},\hat{\eta}) &= \frac{2(1-\lambda_0)}{\pi}\frac{\hat{\eta}_{\mathrm{T}}+\hat{\eta}}{\hat{\xi}^2+(\hat{\eta}_{\mathrm{T}}+\hat{\eta})^2},\quad \hat{Y}_{\hat{\eta},1}(\hat{\xi},\hat{\eta}) = \lambda_0,\\
\hat{Y}_{\hat{\xi},0}(\hat{\xi},\hat{\eta}) &= \frac{2(1-\lambda_0)}{\pi}\frac{\hat{\xi}}{\hat{\xi}^2+(\hat{\eta}_{\mathrm{T}}+\hat{\eta})^2};
\end{aligned} \tag{59}$$

the Lamé coefficient function,

$$\begin{aligned}
\mathcal{G}(\xi,\eta) &= \frac{1}{\delta(\epsilon)}\hat{\mathcal{G}}(\hat{\xi},\hat{\eta},\epsilon) \sim \frac{1}{\delta(\epsilon)}\hat{\mathcal{G}}_0(\hat{\xi},\hat{\eta}) + \cdots,\\
\hat{\mathcal{G}}_0(\hat{\xi},\hat{\eta}) &= \frac{2(1-\lambda_0)}{\pi}\frac{1}{\sqrt{\hat{\xi}^2+(\hat{\eta}_{\mathrm{T}}+\hat{\eta})^2}};
\end{aligned} \tag{60}$$

and the curvature function,

$$\begin{aligned}
\mathcal{K}\{\delta(\epsilon)\hat{\eta}_{\mathrm{B}}\} &= -\frac{1}{\hat{\mathcal{G}}_0(\xi,0)}\frac{\partial^2\hat{\eta}_{\mathrm{B}}}{\partial\hat{\xi}^2} + \hat{\mathcal{K}}_0(\hat{\xi},0) + O\big(\hat{\eta}_{\mathrm{B}}\big),\\
\hat{\mathcal{K}}_0(\hat{\xi},0) &= -\frac{\pi}{2(1-\lambda_0)}\frac{\hat{\eta}_{\mathrm{T}}}{\sqrt{\hat{\xi}^2+\hat{\eta}_{\mathrm{T}}^2}},\\
\hat{\mathcal{K}}_0(0) &= \hat{\mathcal{K}}_0(0,0) = -\frac{\pi}{2(1-\lambda_0)}.
\end{aligned} \tag{61}$$

With the root variables, the inner equation is derived as follows:

$$\begin{aligned}
&\frac{\partial^2\hat{C}}{\partial\hat{\xi}^2} + \big[1+\hat{\eta}_{\mathrm{T}}'^2(\hat{\xi})\big]\frac{\partial^2\hat{C}}{\partial\hat{\eta}^2} - 2\hat{\eta}_{\mathrm{T}}'(\hat{\xi})\frac{\partial^2\hat{C}}{\partial\hat{\eta}\partial\hat{\xi}} - \hat{\eta}_{\mathrm{T}}''(\hat{\xi})\frac{\partial\hat{C}}{\partial\hat{\eta}}\\
&\quad + \epsilon W\left\{\hat{Y}_{\hat{\xi}}\frac{\partial\hat{C}}{\partial\hat{\xi}} + \big[\hat{X}_{\hat{\xi}} - \hat{Y}_{\hat{\xi}}\hat{\eta}_{\mathrm{T}}'(\hat{\xi})\big]\frac{\partial\hat{C}}{\partial\hat{\eta}}\right\} = 0.
\end{aligned} \tag{62}$$

The corresponding boundary conditions are the following:

(1) Matching condition: as $\hat{\eta} \to \infty$, $\hat{C} \Longleftrightarrow \mathbb{C}$.

(2) Side-wall condition: at $\hat{\xi} = 0$, $\frac{\partial\hat{C}}{\partial\hat{\xi}} = 0$.

(3) Interface conditions: with the assumption $\hat{\eta}_{\mathrm{B}} \ll 1$, one may make the asymptotic expansions for all the functions in the limit $\hat{\eta} \to 0$. As a result we derive that, at $\hat{\eta} = 0$,

$$\begin{aligned}
\hat{C} + \frac{\partial\hat{C}}{\partial\hat{\eta}}\hat{\eta}_{\mathrm{B}} &= y_* - \epsilon\ln\delta(\epsilon)W\hat{\mathrm{P}}\mathrm{e}\lambda_G\hat{Y}_*\\
&\quad - \epsilon W\hat{\mathrm{P}}\mathrm{e}\lambda_G[\hat{Y}_0 + \delta(\epsilon)\hat{Y}_1 + \cdots]\\
&\quad - \epsilon W\hat{\mathrm{P}}\mathrm{e}\lambda_G\frac{\partial\hat{Y}_0}{\partial\hat{\eta}}\hat{\eta}_{\mathrm{B}} + \frac{\epsilon^2\pi\hat{\Gamma}}{2\mathbb{M}W(1-\lambda_0)}\frac{\hat{\eta}_{\mathrm{T}}}{\sqrt{\hat{\xi}^2+\hat{\eta}_{\mathrm{T}}^2}}\\
&\quad + \frac{\epsilon^2\hat{\Gamma}}{\mathbb{M}W\hat{\mathcal{G}}_0(\xi,0)}\frac{\partial^2\hat{\eta}_{\mathrm{B}}}{\partial\hat{\xi}^2} + \mathcal{O}\big(\hat{\eta}_{\mathrm{B}}^2\big),
\end{aligned} \tag{63}$$

and

$$\begin{aligned}
&\frac{\partial\hat{C}}{\partial\hat{\eta}} + \frac{\partial^2\hat{C}}{\partial\hat{\eta}^2}\hat{\eta}_{\mathrm{B}} - \frac{\partial\hat{\eta}_{\mathrm{B}}}{\partial\hat{\xi}}\frac{\partial\hat{C}}{\partial\hat{\xi}} - \epsilon W(1-\kappa)\\
&\quad\times\left(\hat{C} + \frac{\partial\hat{C}}{\partial\hat{\eta}}\hat{\eta}_{\mathrm{B}} + \cdots\right)\left(\hat{Y}_{\hat{\xi},0}\frac{\partial\hat{\eta}_{\mathrm{B}}}{\partial\hat{\xi}} - \hat{Y}_{\hat{\eta},0}\right)\\
&\quad + \epsilon W(1-\kappa)\left(\hat{C} + \frac{\partial\hat{C}}{\partial\hat{\eta}}\hat{\eta}_{\mathrm{B}} + \cdots\right)\hat{Y}_{\hat{\eta}\hat{\eta},0}\hat{\eta}_{\mathrm{B}}\\
&\quad + \mathcal{O}\big(\hat{\eta}_{\mathrm{B}}^2\big) = 0.
\end{aligned} \tag{64}$$

The above inhomogeneous system may have the following general form of asymptotic expansions:

$$\begin{aligned}
\hat{C}(\hat{\xi},\hat{\eta},\epsilon) &= (\mathrm{I}) + (\mathrm{II}) = \bar{C}_*(\hat{\xi},\hat{\eta},\epsilon) + \tilde{C}_{\mathrm{s}*}(\hat{\xi},\hat{\eta},\epsilon),\\
\hat{\eta}_{\mathrm{B}}(\hat{\xi},\epsilon) &= (\mathrm{I}) + (\mathrm{II}) = 0 + \tilde{h}_{\mathrm{s}*}(\hat{\xi},\epsilon).
\end{aligned} \tag{65}$$

Part I, $\{\bar{C}_*(\hat{\xi},\hat{\eta},\epsilon),\bar{h}_*(\hat{\xi},\epsilon) = 0\}$, is a particular solution of the inhomogeneous system, which may be expanded in the RPE form. Part II, $\{\tilde{C}_{\mathrm{s}*}(\hat{\xi},\hat{\eta},\epsilon),\tilde{h}_{\mathrm{s}*}(\hat{\xi},\epsilon)\}$, is the general solution of

the associated homogeneous system, which may be expanded in the SPE form.

A. The regular perturbed expansion of the solution in the root region

We find that the RPE part of the solution can be written in the form of multiple variables, $\bar{C}_*(\hat{\xi},\hat{\eta},\epsilon)=\bar{\mathbb{C}}_*(\hat{\xi},\hat{\eta},\bar{\eta}_+,\epsilon)$, with the fast variable defined as $\bar{\eta}_+=\hat{\eta}/\epsilon$ as follows:

$$\bar{\mathbb{C}}_*\sim\bar{\mathbb{C}}_{*0}(\hat{\xi},\hat{\eta},\epsilon)+\epsilon\bar{\mathbb{C}}_{*1}(\hat{\xi},\hat{\eta})+\epsilon^2\bar{\mathbb{C}}_{*2}(\hat{\xi},\hat{\eta},\bar{\eta}_+)+(\text{h.o.t}), \tag{66}$$

where

$$\begin{aligned}\bar{\mathbb{C}}_{*0}&=y_{*0}-\epsilon\ln\delta(\epsilon)W\lambda_G\hat{Y}_*,\\ \bar{\mathbb{C}}_{*1}&=y_{*1}-W\lambda_G\hat{Y}_0(\hat{\xi},\hat{\eta}),\\ \bar{\mathbb{C}}_{*2}&=y_{*02}+\bar{\mathbb{b}}_{2,0}(\hat{\xi},\hat{\eta})+\bar{\mathbb{b}}_{2,1}(\hat{\xi},\hat{\eta})\bar{\eta}_+,\cdots.\end{aligned} \tag{67}$$

The above RPE solution in the root region is fully determined. The solution for $\bar{\mathbb{C}}_*(\hat{\xi},\hat{\eta},\bar{\eta}_+,\epsilon)$ matches well with the RPE part of the outer solution in the limit of $\hat{\xi}\to\infty$ along the paths $\hat{\eta}=A\hat{\xi}^{\alpha}$, $(\mathbb{a}_0\leqslant A<\infty)$. This RPE solution, however, gives no information on the interface shape function nor the parameter $\hat{\xi}_*$.

In order to determine the parameter $\hat{\xi}_*$, we need to derive the SPE part of the solution in the root region from the associated homogeneous system.

B. The singular perturbation expansion of the solution in the root region

The SPE part of the inner solution in the root region also has multiple length scales. To solve the associated homogeneous system of (62)–(64), we introduce the following fast inner variables:

$$\begin{cases}\tilde{\xi}_+=\frac{\tilde{\phi}(\hat{\xi},\hat{\eta})}{\tilde{\beta}(\epsilon)}=\frac{1}{\tilde{\beta}(\epsilon)}\int_0^{\hat{\xi}}\tilde{k}(\hat{\xi}_1,\hat{\eta})\,d\hat{\xi}_1,\\ \tilde{\eta}_+=\frac{\tilde{\psi}(\hat{\xi},\hat{\eta})}{\tilde{\beta}(\epsilon)}=\frac{1}{\tilde{\beta}(\epsilon)}\int_0^{\hat{\eta}}\tilde{k}(\hat{\xi},\hat{\eta}_1)\,d\hat{\eta}_1,\end{cases} \tag{68}$$

and assume that $\tilde{\phi}_{\hat{\xi}}=\sqrt{1+\hat{\eta}_{\mathrm{T}}'^2}\,\tilde{\psi}_{\hat{\eta}}=\tilde{k}(\hat{\xi},\hat{\eta})$, $\tilde{\psi}_{\hat{\xi}}=-\sqrt{1+\hat{\eta}_{\mathrm{T}}'^2}\,\tilde{\phi}_{\hat{\eta}}=\tilde{g}(\hat{\xi},\hat{\eta})$. In terms of these multiple variables $(\hat{\xi},\hat{\eta},\tilde{\xi}_+,\tilde{\eta}_+)$, we write the SPE solution as

$$\tilde{C}_{s*}(\hat{\xi},\hat{\eta},\epsilon)=\tilde{\mathbb{C}}_*(\hat{\xi},\hat{\eta},\tilde{\xi}_+,\tilde{\eta}_+,\epsilon),\quad \tilde{h}_{s*}(\hat{\xi},\epsilon)=\tilde{h}_*(\hat{\xi},\tilde{\xi}_+,\epsilon).$$

As a consequence, the complete inner solution is expressed as

$$\hat{C}(\hat{\xi},\hat{\eta},\epsilon)=\bar{\mathbb{C}}_*(\hat{\xi},\hat{\eta},\bar{\eta}_+,\epsilon)+\tilde{\mathbb{C}}_*(\hat{\xi},\hat{\eta},\tilde{\xi}_+,\tilde{\eta}_+,\epsilon). \tag{69}$$

The system (62)–(64) can be converted into the system with the multiple variables $(\hat{\xi},\hat{\eta},\tilde{\xi}_+,\tilde{\eta}_+)$ as follows:

$$(\tilde{k}^2+\tilde{g}^2)\left(\frac{\partial^2}{\partial\tilde{\xi}_+^2}+\frac{\partial^2}{\partial\tilde{\eta}_+^2}\right)\tilde{\mathbb{C}}_*+O[\tilde{\beta}(\epsilon)]=0. \tag{70}$$

The boundary conditions are the following;

(1) Matching condition: as $\hat{\eta}\to\infty$ and $\hat{\xi}\to\infty$,

$$\begin{aligned}&\hat{C}_*(\hat{\xi},\hat{\eta},\tilde{\xi}_+,\tilde{\eta}_+,\epsilon)=\tilde{\mathbb{C}}_*(\hat{\xi},\hat{\eta},\tilde{\xi}_+,\tilde{\eta}_+,\epsilon)+\bar{\mathbb{C}}_*(\hat{\xi},\hat{\eta},\bar{\eta}_+,\epsilon),\\ &\Updownarrow\\ &C_{\mathrm{B}}(\xi,\eta,\epsilon)=c_*-\epsilon W\lambda_G\hat{Y}_0+\epsilon^2\bar{\mathbb{C}}_2(\hat{\xi},\hat{\eta},\epsilon)+\cdots\\ &\quad+\tilde{\mathbb{C}}(\xi,\eta,\xi_+,\eta_+,\varepsilon)+\cdots.\end{aligned} \tag{71}$$

(2) The interface conditions: with the multiple variables defined above and the formula (69), the interface conditions (63) and (64) are converted in the following forms: at the interface $\hat{\eta}=\tilde{\eta}_+=0$,

$$\begin{aligned}&\tilde{\mathbb{C}}_*+\left(\frac{1}{\varepsilon}\frac{\partial\bar{\mathbb{C}}_*}{\partial\bar{\eta}_+}+\frac{\partial\bar{\mathbb{C}}_*}{\partial\hat{\eta}}\right)\tilde{h}_*=-\epsilon W\lambda_G\frac{\partial\hat{Y}_0}{\partial\hat{\eta}}\tilde{h}_*\\ &\quad+\frac{\epsilon^2\hat{\Gamma}\tilde{k}^2}{\tilde{\beta}^2\mathbb{M}W\hat{\mathcal{G}}_0(\xi,0)}\frac{\partial^2\tilde{h}_*}{\partial\tilde{\xi}_+^2}+\cdots\end{aligned} \tag{72}$$

and

$$\begin{aligned}&\left(\frac{\partial\tilde{\mathbb{C}}_*}{\partial\hat{\eta}}+\frac{\tilde{k}}{\tilde{\beta}\sqrt{1+\hat{\eta}_{\mathrm{T}}'^2}}\frac{\partial\tilde{\mathbb{C}}_*}{\partial\tilde{\eta}_+}\right)+\left(\frac{\partial^2\bar{\mathbb{C}}_*}{\partial\hat{\eta}^2}+\frac{2}{\varepsilon}\frac{\partial^2\bar{\mathbb{C}}_*}{\partial\bar{\eta}_+\partial\hat{\eta}}\right.\\ &\left.+\frac{1}{\varepsilon^2}\frac{\partial^2\bar{\mathbb{C}}_*}{\partial\bar{\eta}_+^2}\right)\tilde{h}_*-\left(\frac{\tilde{k}}{\tilde{\beta}}\frac{\partial\tilde{h}_*}{\partial\tilde{\xi}_+}+\frac{\partial\tilde{h}_*}{\partial\hat{\xi}}\right)\frac{\partial\bar{\mathbb{C}}_*}{\partial\hat{\xi}}\\ &-\epsilon W(1-\kappa)\bar{\mathbb{C}}_*\hat{Y}_{\hat{\xi},0}\left(\frac{\tilde{k}}{\tilde{\beta}}\frac{\partial\tilde{h}_*}{\partial\tilde{\xi}_+}+\frac{\partial\tilde{h}_*}{\partial\hat{\xi}}\right)\\ &+\epsilon W(1-\kappa)\bar{\mathbb{C}}_*\hat{Y}_{\hat{\eta},0}+\epsilon W(1-\kappa)\hat{Y}_{\hat{\eta},0}\frac{\partial\bar{\mathbb{C}}_*}{\partial\hat{\eta}}\tilde{h}_*\\ &+\epsilon W(1-\kappa)\bar{\mathbb{C}}_*\hat{Y}_{\hat{\eta}\hat{\eta},0}\tilde{h}_*+\mathcal{O}(\text{h.o.t.})=0.\end{aligned} \tag{73}$$

Make the following asymptotic expansion (SPE) in the limit of $\epsilon\to0$:

$$\begin{aligned}\tilde{\mathbb{C}}_*(\hat{\xi},\hat{\eta},\tilde{\xi}_+,\tilde{\eta}_+,\epsilon)&=\tilde{\mu}_{*0}(\epsilon)\tilde{\mathbb{C}}_{*0}(\hat{\xi},\hat{\eta},\tilde{\xi}_+,\tilde{\eta}_+)\\ &\quad+\tilde{\mu}_{*1}(\epsilon)\tilde{\mathbb{C}}_{*1}(\hat{\xi},\hat{\eta},\tilde{\xi}_+,\tilde{\eta}_+)+\cdots\\ \tilde{h}_*(\hat{\xi},\tilde{\xi}_+,\epsilon)&=\tilde{b}_{*0}(\epsilon)\tilde{h}_{*0}(\hat{\xi},\tilde{\xi}_+)+\tilde{b}_{*1}(\epsilon)\tilde{h}_{*1}(\hat{\xi},\tilde{\xi}_+)\\ &\quad+\cdots,\end{aligned} \tag{74}$$

where the asymptotic factors $1\gg\tilde{\mu}_{*0}(\epsilon)\gg\tilde{\mu}_{*1}(\epsilon)\gg\cdots$ and $1\gg\tilde{b}_{*0}(\epsilon)\gg\tilde{b}_{*1}(\epsilon)\gg\cdots$ are to be determined. Furthermore, let

$$\begin{aligned}\tilde{k}(\hat{\xi},\hat{\eta},\epsilon)&=\tilde{k}_0(\hat{\xi},\hat{\eta})+\epsilon\tilde{k}_1(\hat{\xi},\hat{\eta})+\cdots,\\ \tilde{g}(\hat{\xi},\hat{\eta},\epsilon)&=\tilde{k}_0(\hat{\xi},\hat{\eta})+\epsilon\tilde{g}_1(\hat{\xi},\hat{\eta})+\cdots.\end{aligned} \tag{75}$$

By substituting the above to the system (70)-(73), one can derive each order approximation, successively. We are interested only in the leading-order approximation solution, so we may take $\bar{\mathbb{C}}_*\approx y_{*0}-W\lambda_G\epsilon\ln\delta(\epsilon)\hat{Y}_*+\epsilon[y_{*1}-W\lambda_G\hat{Y}_0(\hat{\xi},\hat{\eta})]$.

C. The zeroth-order approximation $O[\tilde{\mu}_{*0}(\epsilon)]$

To balance the leading terms in (73), it is derived that

$$\tilde{\beta}=O(\epsilon^{\frac{1}{2}}),\quad \tilde{\mu}_{*0}(\epsilon)=\epsilon\tilde{b}_{*0}(\epsilon). \tag{76}$$

Let $\tilde{\beta}=\sqrt{\epsilon\hat{\Gamma}}$. As a consequence, we have the equation:

$$\frac{\partial^2\tilde{\mathbb{C}}_{*0}}{\partial\tilde{\xi}_+^2}+\frac{\partial^2\tilde{\mathbb{C}}_{*0}}{\partial\tilde{\eta}_+^2}=0, \tag{77}$$

and the following boundary conditions:

(1) Matching condition: as $\hat{\eta}\to\infty$ and $\xi\to-1$, $\eta\to0$, $\tilde{\mathbb{C}}_{*0}\Longleftrightarrow\tilde{C}_0$.

(2) Symmetry condition about $\hat{\xi}=0$:

$$\tilde{\mathbb{C}}_{*0}(\hat{\xi},\hat{\eta},\tilde{\xi}_+,\tilde{\eta}_+)=\tilde{\mathbb{C}}_{*0}(-\hat{\xi},\hat{\eta},-\tilde{\xi}_+,\tilde{\eta}_+).$$

(3) The interface conditions at the interface, $\hat{\eta} = \tilde{\eta}_+ = 0$: With the notation $\tilde{k}_0(\hat{\xi},0) = \hat{k}_0(\hat{\xi})$,

$$\tilde{\mathbb{C}}_{*0} = \frac{\hat{k}_0^2}{\mathbb{M}W\hat{\mathcal{G}}_0(\hat{\xi},0)}\frac{\partial^2\tilde{h}_{*0}}{\partial\tilde{\xi}_+^2},$$

$$\frac{\hat{k}_0}{\sqrt{1+\hat{\eta}_{\mathrm{T}}'^2}}\frac{\partial\tilde{\mathbb{C}}_{*0}}{\partial\tilde{\eta}_+} - \hat{k}_0 W[(1-\kappa)y_{*0} - \lambda_{\mathrm{G}}] \times \hat{Y}_{\hat{\xi},0}(\hat{\xi},0)\frac{\partial\tilde{h}_{*0}}{\partial\tilde{\xi}_+} = 0. \tag{78}$$

The system allows the normal modes solutions:

$$\tilde{\mathbb{C}}_{*0} = \tilde{A}_{*0}(\xi,\eta)\exp(\mathrm{i}\tilde{\xi}_+ - \tilde{\eta}_+), \quad \tilde{h}_{*0} = \tilde{D}_{*0}\exp(\mathrm{i}\tilde{\xi}_+), \tag{79}$$

where $\tilde{D}_{*0}$ is a constant. In order to satisfy the interface conditions (78) the function $\hat{k}_0(\hat{\xi})$ is subjected to the formula:

$$\frac{\hat{k}_0^3}{\mathbb{M}W\hat{\mathcal{G}}_0(\hat{\xi},0)\sqrt{1+\hat{\eta}_{\mathrm{T}}'^2}} - \mathrm{i}\hat{k}_0 W\hat{Y}_{\hat{\xi},0}(\hat{\xi},0) \times [(1-\kappa)y_{*0} - \lambda_{\mathrm{G}}] = 0. \tag{80}$$

Similar to the SPE solution in the outer region, there are three roots for $\hat{k}_0$:

$$\hat{k}_0^{(1)}(\hat{\xi}) = \hat{k}_s(\hat{\xi}),\ \hat{k}_0^{(2)}(\hat{\xi}) = -\hat{k}_s(\hat{\xi}),\ \hat{k}_0^{(3)}(\hat{\xi}) = 0, \tag{81}$$

where $\hat{k}_s(\hat{\xi}) = e^{\frac{\mathrm{i}\pi}{4}}\hat{\mathbb{m}}\sqrt{\hat{\mathcal{G}}_0(\hat{\xi},0)\hat{Y}_{\hat{\xi},0}(\hat{\xi},0)}(1+\hat{\eta}_{\mathrm{T}}'^2)^{\frac{1}{4}}$, and $\hat{\mathbb{m}} = W\sqrt{\mathbb{M}[(1-\kappa)y_{*0} - \lambda_{\mathrm{G}}]}$. With the formulas

$$\begin{cases}\hat{\mathcal{G}}_0(\hat{\xi},0) = \frac{2(1-\lambda_0)}{\pi}\frac{\hat{\eta}_{\mathrm{T}}(\hat{\xi})}{\sqrt{\hat{\xi}^2+\hat{\eta}_{\mathrm{T}}^2(\hat{\xi})}} \\ \hat{Y}_{\hat{\xi},0}(\hat{\xi},0) = \frac{2(1-\lambda_0)}{\pi}\frac{\hat{\xi}}{\hat{\xi}^2+\hat{\eta}_{\mathrm{T}}^2(\hat{\xi})} > 0, (0 \leqslant \hat{\xi} < \infty),\end{cases} \tag{82}$$

one may write three fundamental solutions in the form

$$\hat{H}_1(\hat{\xi}) = e^{\frac{\mathrm{i}}{\sqrt{\epsilon\hat{\Gamma}}}\hat{\chi}(\hat{\xi})},\ \hat{H}_2(\xi) = e^{-\frac{\mathrm{i}}{\sqrt{\epsilon\hat{\Gamma}}}\hat{\chi}(\hat{\xi})},\ \hat{H}_3(\hat{\xi}) = 1, \tag{83}$$

where

$$\hat{\chi}(\hat{\xi}) = \int_{\hat{\xi}_*}^{\hat{\xi}}\hat{k}_s(\hat{\xi}_1)\,d\hat{\xi}_1 = \hat{\chi}_{\mathrm{R}}(\xi) + \mathrm{i}\hat{\chi}_{\mathrm{I}}(\hat{\xi}) = (1+\mathrm{i})\frac{\sqrt{2}\hat{\mathbb{m}}(1-\lambda_0)}{\pi}\int_{\hat{\xi}_*}^{\hat{\xi}}\frac{\hat{\xi}_1^{\frac{1}{2}}\left(1+\hat{\eta}_{\mathrm{T}}'^2\right)^{\frac{1}{4}}}{\left[\hat{\xi}_1^2+\hat{\eta}_{\mathrm{T}}^2(\hat{\xi}_1)\right]^{\frac{3}{4}}}d\hat{\xi}_1. \tag{84}$$

It is seen that in the region $(\hat{\xi}_* \leqslant \hat{\xi} < \infty)$, $\mathrm{Re}[\hat{k}_s(\hat{\xi})] > 0$, $\mathrm{Im}[\hat{k}_s(\hat{\xi})] > 0$, so that

$$\begin{cases}\mathrm{Re}\left[\hat{k}_0^{(1)}(\hat{\xi})\right] > 0, \quad \mathrm{Im}\left[\hat{k}_0^{(1)}(\hat{\xi})\right] > 0; \\ \mathrm{Re}\left[\hat{k}_0^{(2)}(\hat{\xi})\right] < 0, \quad \mathrm{Im}\left[\hat{k}_0^{(2)}(\hat{\xi})\right] < 0.\end{cases}$$

It is deduced that the solution $\hat{H}_2$ is dominant, increasing exponentially as $\hat{\xi} \to \infty$; while the solution $\hat{H}_1$ is subdominant, deceasing exponentially as $\hat{\xi} \to \infty$, The general inner solution can be written in the form

$$\tilde{h}_{*0}(\hat{\xi},\tilde{\xi}_+) = \tilde{d}_1\hat{H}_1(\hat{\xi}) + \tilde{d}_2\hat{H}_2(\hat{\xi}) + \tilde{d}_3\hat{H}_3(\hat{\xi}). \tag{85}$$

D. Root solution in subregion I and the match condition with the outer solution

To match the root solution in the section of $(\hat{\xi} > \hat{\xi}_*)$ with the outer solution in the limits $\hat{\xi} \to \infty$ and $\xi \to -1$, one must set the constants $\tilde{d}_1 = \tilde{d}_3 = 0$, and $\tilde{d}_2 = \Delta(\epsilon)h_1(0)$ in (85), where

$$\Delta(\epsilon) = \exp\left\{-\frac{(1-\mathrm{i})}{\sqrt{\epsilon\hat{\Gamma}}}\frac{\sqrt{2}\hat{\mathbb{m}}(1-\lambda_0)}{\pi} \times \int_{\hat{\xi}_*}^{\frac{1}{\delta}}\frac{\hat{\xi}_1^{\frac{1}{2}}\left[1+\hat{\eta}_{\mathrm{T}}'^2(\hat{\xi}_1)\right]^{\frac{1}{4}}}{\left[\hat{\xi}_1^2+\hat{\eta}_{\mathrm{T}}^2(\hat{\xi}_1)\right]^{\frac{3}{4}}}d\hat{\xi}_1\right\}$$

is a transcendentally small factor. As a result, the SPE part of the root solution in subsection (I) is obtained as

$$\delta(\epsilon)\tilde{h}_{*0} = \epsilon\Delta(\epsilon)h_1(0)\hat{H}_2(\hat{\xi}) + \cdots. \tag{86}$$

E. Root solution in subregion II and quantization condition

The SPE part of the root solutions in subregion II, $(0 < \hat{\xi} < \hat{\xi}_*)$, may be expressed as

$$\tilde{h}_{*0}(\hat{\xi}) = \tilde{d}_1\hat{H}_1(\hat{\xi}) + \tilde{d}_2\hat{H}_2(\hat{\xi}), \tag{87}$$

which are subjected to the following conditions:

(1) The root smoothness conditions at $(\hat{\xi} = 0, \hat{\eta} = \hat{\eta}_{\mathrm{b}})$:

$$\tilde{h}_{*0}(0) = 0, \quad \tilde{h}_{*0}'(0) = 0. \tag{88}$$

(2) The match condition with the solution in sub-inner region I:

$$\delta(\epsilon)\tilde{h}_{*0} \sim \epsilon\Delta(\epsilon)h_1(0)\hat{H}_2(\hat{\xi}). \tag{89}$$

The problem under study is similar to the problem of Schrödinger waves trapped in a finite potential well over the interval $(0 \leqslant \hat{\xi} < \hat{\xi}_*)$ in the quantum mechanics as sketched in Fig. 11. Here, with the general form of the solution (87), the problem for us is to determine the connection condition of the pair of coefficients $\{\tilde{d}_1, \tilde{d}_2\}$ with the coefficient $\epsilon\Delta(\epsilon)h_1(0)$. The root system, as indicated before, has singularity at $\hat{\xi} = \hat{\xi}_*$, as the functions $\hat{\eta}_{\mathrm{T}}(\hat{\xi})$ and $\hat{k}_s(\hat{\xi})$ have a higher-order discontinuity there. It can be further proven that $\hat{\xi} = \hat{\xi}_*$ is a simple turning point of the system in the root region, and there is a transition region with the thickness $\epsilon^{1/3}$ in the vicinity of $\hat{\xi}_*$ between root subregion I and II. This region is root subregion III. In the leading-order approximation the governing equation for the interface shape in this transition region can be reduced

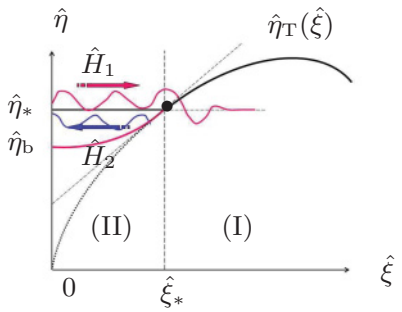

FIG. 11. (Color online) The sketch of wave diagram with W-wave representation in the root region.

to the Airy equation. The inner solution in the transition region must match with the inner solution in the subregion (I) on the right side, while match the inner solution in subregion (II) on the left hand side. These matching conditions lead to the connection condition:

$$\tilde{d}_2 = \epsilon\Delta(\epsilon)h_1(0), \quad \tilde{d}_1 = -\mathrm{i}\tilde{d}_2; \tag{90}$$

consequently, the inner solution (87) in subregion II, ($0 \leqslant \hat{\xi} \leqslant \hat{\xi}_*$):

$$\tilde{h}_{*0}(\hat{\xi}) = \epsilon\Delta(\epsilon)h_1(0)\mathrm{Re}[\hat{H}_2(\hat{\xi}) - \mathrm{i}\hat{H}_1(\hat{\xi})]. \tag{91}$$

One may now apply the root smoothness conditions (88) to the solution (91). Due to $H_1'(0) = H_2'(0) = 0$, the smoothness condition $\tilde{h}'_{*0}(0) = 0$ is always satisfied. The condition $\tilde{h}_{*0}(0) = \mathrm{Re}[\hat{H}_2(0) - \mathrm{i}\hat{H}_1(0)] = 0$ results in the quantization condition:

$$\frac{Q_c(\hat{\xi}_*)}{\mathbb{A}\sqrt{\epsilon\hat{\Gamma}}} = q_n, \quad (n = 0,1,2,\ldots), \tag{92}$$

where $0 < q_0 < q_1 < q_2 < \cdots$ are solutions of the equation: $e^{2\hat{Q}} = \cot\hat{Q}$, and

$$\mathbb{A} = \frac{\pi}{\sqrt{2}\mathbb{m}(1-\lambda_0)}, \quad Q_c(\hat{\xi}_*) = \int_0^{\hat{\xi}_*} \frac{\hat{\xi}_1^{\frac{1}{2}}\left[1+\hat{\eta}_{\mathrm{T}}'^2(\hat{\xi}_1)\right]^{\frac{1}{4}}}{\left[\hat{\xi}_1^2+\hat{\eta}_{\mathrm{T}}^2(\hat{\xi}_1)\right]^{\frac{3}{4}}}\, d\hat{\xi}_1.$$

The numerical computations show that $q_0 = 0.4128, q_1 = 3.1434, q_2 = 6.2832, \cdots$, and $q_n \approx n\pi$ as $n \gg 1$. From the quantization condition (92) one obtains a discrete set of eigenvalues $\hat{\xi}_*$ with index $n = 0,1,2,\ldots$:

$$\hat{\xi}_* = \{\hat{\xi}_*^{(0)} < \hat{\xi}_*^{(1)} < \hat{\xi}_*^{(2)}, \cdots\},$$

as the function of ϵ and other parameters of the system. The calculations show that for a large n, the corresponding eigenvalue $\hat{\xi}_*^{(n)}$ will be very large, so that it should be ruled out. The variations of the smallest eigenvalue $\hat{\xi}_* = \hat{\xi}_*^{(0)}$ with ϵ are shown in Fig. 12 for $\hat{\Gamma} = 1.0, 1.5, 2.0$, and other typical parameters: $\lambda_G = 2.0, \kappa = 0.1, \lambda_0 = 0.6, W_0 = 1.7453, \mathbb{M} = 1.0$. From the outer solutions in these cases, we calculated that

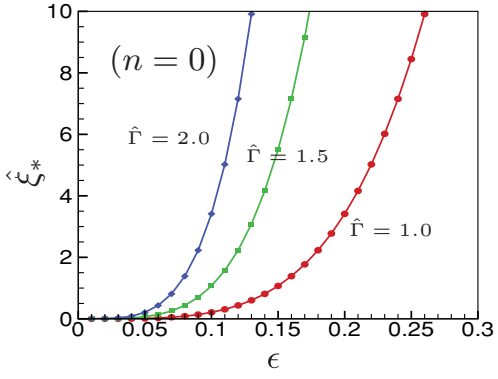

FIG. 12. (Color online) The variations of $\hat{\xi}_*$ with the parameter ϵ for the cases: $\lambda_G = 2.0$, $\kappa = 0.1$, $\lambda_0 = 0.6$, $W_0 = 1.7453$, $\mathbb{M} = 1.0$, and $\hat{\Gamma} = 1.0, 1.5, 2.0$ and $n = 0$. It is calculated from the outer solutions for these cases that $\alpha = 0.88$ and $\mathbb{a}_0 = 2.63$.

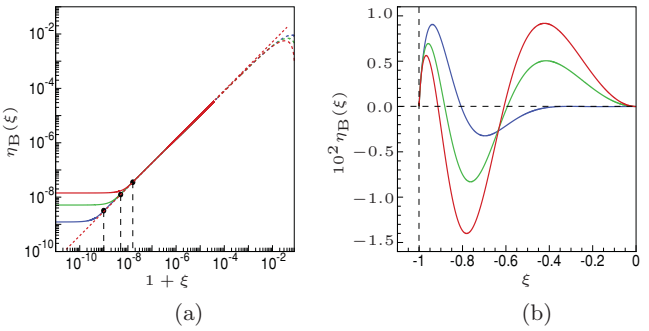

FIG. 13. (Color online) The graph of composite solution $\eta_B(\xi)$ in $(\hat{\xi},\hat{\eta})$ plane for the typical case: $\epsilon = 0.1, \kappa = 0.1, \lambda_G = 2.0, \lambda_0 = 0.6$, $\mathbb{M} = 1.0$. (a) The graphs of the solutions $\eta_B(\xi)$ near $\xi = -1$ for $\hat{\Gamma} = 1.0, 1.5, 2.0$ from bottom to top on the left-hand side of the figure. The bullets show the transition points in the root region. (b) The graphs of solutions $\eta_B(\xi)$ over $(-1 < \xi \leqslant 0)$ for $\hat{\Gamma} = 1.0, 1.5, 2.0$ from bottom to top on the right-hand side of the figure. It is calculated from the outer solutions for these cases that $\alpha = 0.88$, $\mathbb{a}_0 = 2.63$, and $\delta(\epsilon) = 0.4642 \times 10^{-8}$.

$\alpha = 0.88$ and $\mathbb{a}_0 = 2.63$ and found that the numerical values of α and $\mathbb{a}_0$ are rather insensitive to the variation of parameter $\hat{\Gamma}$. It is seen from the figure that $\hat{\xi}_*$ increases with creasing surface tension parameter $\hat{\Gamma}$ and Péclet number ϵ.

Once $\hat{\xi}_*$ is determined, the parameters $\hat{\eta}_*$ and $\hat{\eta}_b$, as well as the inner solution in the whole root region ($0 \leqslant \hat{\xi} < \infty$) are determined, which may be written as

$$\hat{\eta}_B(\hat{\xi},\epsilon) = \delta(\epsilon)\hat{\eta}_T(\hat{\xi}) + \epsilon\Delta(\epsilon)h_1(0)e^{\frac{\hat{\chi}_I(\hat{\xi})}{\sqrt{\epsilon\hat{\Gamma}}}}\cos\left[\frac{\hat{\chi}_R(\hat{\xi})}{\sqrt{\epsilon\hat{\Gamma}}}\right] + \cdots. \tag{93}$$

Combining with the outer solution

$$\eta_B(\xi,\epsilon) = \epsilon\left\{h_1(\xi) - h_1(0)e^{\frac{\chi_I(\xi)}{\sqrt{\epsilon\hat{\Gamma}}}}\cos\left[\frac{\chi_R(\xi)}{\sqrt{\epsilon\hat{\Gamma}}}\right]\right\} + \cdots, \tag{94}$$

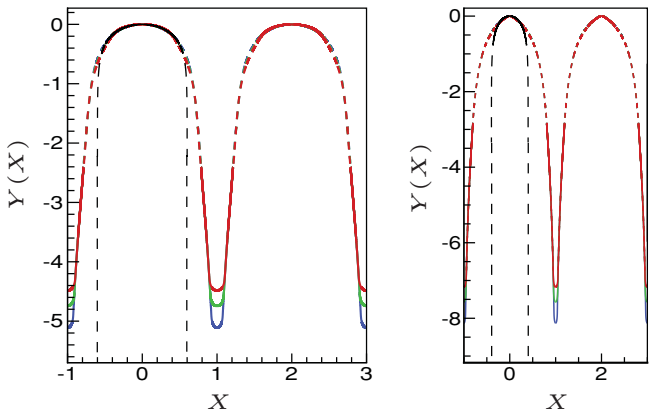

FIG. 14. (Color online) The interface shapes described on (X,Y) plane for the typical case: $\kappa = 0.1$, $\mathbb{M} = 1.0$, and (a) $\lambda_0 = 0.6$, $\lambda_G = 2.0$, $\hat{\Gamma} = 1.0, 1.5, 2.0$ for the mode $n = 0$; the solid line is given by the root solution from bottom to top. (b) $\lambda_0 = 0.4$, $\lambda_G = 0.8$, $\hat{\Gamma} = 2.0, 3.0, 4.0$ for the mode $n = 0$ from bottom to top. In the figures, the black dashed line is given by the ST solution.

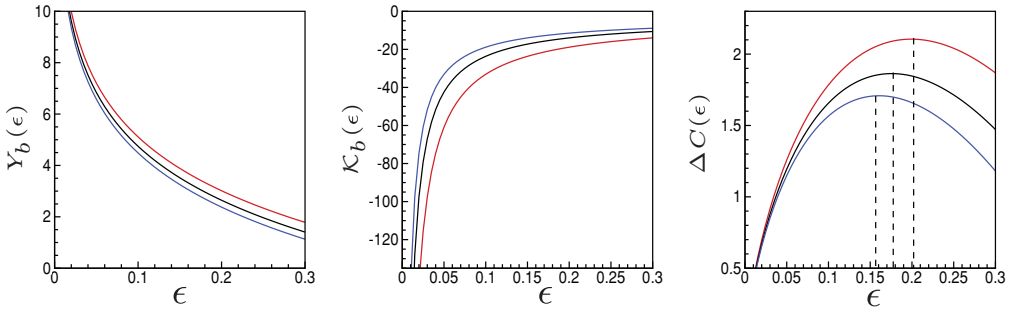

FIG. 15. (Color online) The properties of cellular growth at the bottom of the root for the typical case: $\kappa = 0.1$, $\lambda_G = 2.0$, $\lambda_0 = 0.6$, $\mathbb{M} = 1.0$, and cases $\hat{\Gamma} = 1.0, 1.5, 2.0$: (a) The total lengths of finger from top to bottom; (b) the mean curvature of the bottom of the root for from bottom to top; (c) the difference of the concentrations of impurity at the bottom from that at the tip, from top to bottom. It has a maximum value as $\epsilon = 0.1565, 0.1776, 0.2020$ correspondingly.

one may write the composite solution as

$$\eta_B(\xi,\epsilon) = \delta(\epsilon)\hat{\eta}_T(\hat{\xi}) - \epsilon \mathbb{a}_0(1+\xi)^\alpha + \epsilon\left\{h_1(\xi) - h_1(0)e^{\frac{\chi_I(\xi)}{\sqrt{\epsilon\hat{\Gamma}}}}\cos\left[\frac{\chi_R(\xi)}{\sqrt{\epsilon\hat{\Gamma}}}\right]\right\} + \cdots. \tag{95}$$

The composite solutions for the interface shape function $\eta_B(\xi)$ for the cases $\hat{\Gamma} = 0.5$, 1.5, 2.0 are shown in Fig. 13(a)–13(b), respectively. The global interface shape on the (X,Y) plane for the cases of $\lambda_0 = 0.6$ and $\lambda_0 = 0.4$ and different values of parameter $\hat{\Gamma}$ are shown in Fig. 14(a) and 14(b), respectively. In the figure, for the comparisons we have also shown the ST solution with a black dashed line and the outer solution with a solid red line. It is seen that the feature of the global interface shape of cell in the physical plane (x,y) is quite different from the shape of the ST finger. Nevertheless, the global interface shape of the cell and the interface shape of the ST finger are very close to each other in the (ξ,η) plane as $\epsilon \to 0$, as is pointed out at the beginning of the paper. It is also seen that in the physical (x,y) plane, away from the bottom of the root, the global solution is very close to the outer solution, while in the root region the global solution modifies the feature of outer solution significantly, due to the effect of the isotropic surface tension.

Moreover, in terms of the above root solution, we may derive the total length of the finger:

$$Y_b = |Y(-1,\delta(\epsilon)\hat{\eta}_b)| \approx |\ln\delta(\epsilon)\hat{Y}_* + \hat{Y}_0(0,\hat{\eta}_b)| = \frac{2(1-\lambda_0)}{\pi}\left|\ln\delta(\epsilon) + \ln\left(\frac{\pi\hat{\eta}_b}{2}\right)\right|; \tag{96}$$

the mean curvature of the bottom of the root:

$$\mathcal{K}_b \approx -\frac{\pi}{2(1-\lambda_0)}(1 + 2\mathbb{a}_2\hat{\eta}_b); \tag{97}$$

the concentration of impurity at the bottom of the root ($\hat{\xi} = 0, \hat{\eta} = \hat{\eta}_b$):

$$C_{\rm root} = \{[y_{*0} + \epsilon y_{*1} - W\lambda_G\epsilon\ln\delta(\epsilon)\hat{Y}_*] - \epsilon W\lambda_G\hat{Y}_0(0,\hat{\eta}_b) + \cdots\} + \cdots, \tag{98}$$

where $\hat{Y}_0(0,\hat{\eta}_b) = (1-\lambda_0)/\pi\,\ln(\pi^2\hat{\eta}_b^2/4)$, $\hat{Y}_* = 2(1-\lambda_0)/\pi$. Thus, we derive the difference of concentrations of impurity at the bottom of the root from that at the cell tip:

$$\Delta\mathbb{C} = C_{\rm root} - C_{\rm tip} = -\epsilon W\lambda_G\frac{2(1-\lambda_0)}{\pi} \times\left[\ln\delta(\epsilon) + \ln\left(\frac{\pi\hat{\eta}_b}{2}\right)\right]. \tag{99}$$

In Fig. 15(a)–15(c), we show the variations of Y_b, $\mathcal{K}_b$, and $\Delta\mathbb{C}$ with ϵ and $\hat{\Gamma}$ for the typical cases: $\kappa = 0.1$, $\lambda_G = 2.0$, $\lambda_0 = 0.6$, $\mathbb{M} = 1.0$, and $\hat{\Gamma} = 1.0, 1.5, 2.0$. It is seen that as ϵ decreases, the total length of finger increases, while the curvature of the bottom of the root $|\mathcal{K}_b|$ increases, while $\Delta\mathbb{C}$ decreases after passing its maximum value. On the other hand, as surface-tension parameter $\hat{\Gamma}$ increases, the total length of the finger decreases, and the curvature of the bottom of the root $|\mathcal{K}_b|$ decreases, or, say, the radius of curvature at the bottom of the root increases, while $\Delta\mathbb{C}$ decreases.

VI. CONCLUSIONS AND DISCUSSION

In the present paper, we develop a global asymptotic theory for 2D steady deep-cellular growth in solidification with isotropic surface tension. The results obtained show that the system allows a family of steady solutions with two free parameters: the Péclet number ϵ, which depends on the product of tip radius ℓ_t and pulling speed V, and the asymptotic width λ_0, which is relative to the primary spacing W_0. One of the most important results drawn in the present paper is that the global steady-state solutions of cellular growth have a complicated structure with three internal layers in the root region; for given (ϵ,λ_0), there exists a discrete set of the global steady-state solutions subject to the quantization condition (92). Each eigenvalue $\hat{\xi}_*$ calculated from the quantization condition determines the total length of cell. The effect of the surface tension parameter on the steady-state solutions in the outer region is minor with the magnitude $O(\epsilon^2)$. However, it plays a crucial role in the region of the root through the quantization condition. It is shown that the arrayed-cellular growth with a finite closure of the root cannot exist without the isotropic surface tension.

The theoretical predictions for the global interface shapes have been compared quantitatively with the experimental observations made by Georgelin and Pocheau [20,21] under various growth conditions without any adjustable parameter. The agreements between both are very satisfactory. It is seen that the effects of three dimensionality and anisotropy of interface energy, which are neglected in the present model, are insignificant on the interface shapes in the region not close to the bottom of the cell's root.

So far, the experimental data of total length of cell and concentration of impurity at the bottom of the root are not available. Hence, at this moment the quantitative comparisons between the theoretical predictions for these quantities and the corresponding experimental data cannot be further conducted. We anticipate that more complete experimental data for global interface shapes of steady cellular growth will be available in the near future.

Our results based on 2D Hele-Shaw model do not show the formation of liquid droplets in the solid phase near the bottom of the root, which has been observed in the experiments as reported by Kurowski *et al.* [32]. Brattkus [33] proposed a simplified model by considering the groove as an axisymmetric liquid threat. He then found that the groove may break into liquid droplets due to the Rayleigh instability. Our solutions of steady deep-cellular growth for some cases show a long and thin groove, whose width in the root region is compatible with the thickness of the Hele-Shaw cell. As a consequence, the effect of three dimensionality of the Hele-Shaw cell indeed needs to be taken into account. Furthermore, the solute diffusivity in the solid phase, as well as the anisotropy of surface tension, may also play a significant role. Therefore, the liquid-droplet formation and other related phenomena near the bottom of the root cannot be investigated under the current model. In order to explore the mechanism of droplet formation, some additional physical effects need to be taken into account, and a more sophisticated model needs to be established.

ACKNOWLEDGMENTS

The work is supported by Nankai University, China, and partial support is from the University of Science and Technology in Beijing under the "Overseas Distinguished Scholar program" sponsored by the Department of Chinese Education. The authors are very grateful to Prof. S.H. Davis for his valuable suggestions and discussion.

[1] J. W. Rutter and B. Chalmers, Can. J. Phys. **31**, 15 (1953).
[2] W. W. Mullins and R. F. Sekerka, J. Appl. Phys. **34**, 323 (1963).
[3] W. W. Mullins and R. F. Sekerka, J. Appl. Phys. **35**, 444 (1964).
[4] P. Pelcé and A. Pumir, J. Cryst. Growth **73**, 337 (1985).
[5] J. D. Weeks and W. van-Saarloons, Phys. Rev. A **39**, 2772 (1989).
[6] M. Mashaal, M. Ben Amar, and V. Hakim, Phys. Rev. A **41**, 4421 (1990).
[7] J. D. Weeks, W. van-Saarloons, and M. Grant, J. Crystal Growth. **112**, 244 (1991).
[8] B. Caroli, C. Caroli, and B. Roulet, in *Solids Far from Equilibrium*, edited by C. Godreche (Cambridge University Press, Cambridge, UK, 1991), p. 155.
[9] S. H. Davis, *Effect of Flow on Morphological Stability*, in *Handbook of Crystal Growth*, Vol. 1: *Fundamentals, Part B: Transport and Stability*, edited by D. T. J. Hurle (Elsevier Science Publishers, Amsterdam, London, New York, Tokyo, 1993), pp. 859–897.
[10] P. Molho, A. J. Simon, and A. Libchaber, Phys. Rev. A **42**, 904 (1990).
[11] B. Billia and R. Trivedi, in *Handbook of Crystal Growth*, Vol. 1: *Fundamentals, Part B: Transport and Stability*, edited by D. T. J. Hurle (Elsevier Science Publishers, Amsterdam, London, New York, Tokyo, 1993), pp. 899–1073.
[12] K. Somboonsuk, J. T. Mason, and R. Trivedi, Metall. Trans. A **15**, 967 (1984).
[13] R. Trivedi, Metall. Trans. A **15**, 977 (1984).
[14] P. Kopczyncki, W.-J. Rappel, and A. Karma, Phys. Rev. Lett. **77**, 3387 (1996).
[15] M. Losert, D. A. Stillman, H. Z. Cummins, P. Kopczyncki, W.-J. Rappel, and A. Karma, Phys. Rev. E **58**, 7492 (1998).
[16] J. Kageyama1, Y. Sasajima, and M. Ichimura, Metall. Trans. **46**, 2003 (2005).
[17] S. Gurevich and A. Karma, Phys. Rev. E **81**, 011603 (2010).
[18] B. Echebarria, A. Karma, and S. Gurevich, Phys. Rev. E **81**, 021608 (2010).
[19] M. Georgelin and A. Pocheau, J. Cryst. Growth **268**, 272 (2004).
[20] M. Georgelin and A. Pocheau, Phys. Rev. E **73**, 011604 (2006).
[21] A. Pocheau and M. Georgelin, J. Cryst. Growth **206**, 215 (1999).
[22] T. F. Bower, H. D. Brody, and M. C. Flemings, Trans. Metall. Soc. AIME **236**, 624 (1966).
[23] J. J. Xu, Phys. Rev. E **53**, 5031 (1996).
[24] P. G. Saffman and G. I. Taylor, Proc. R. Soc. London A **245**, 312 (1958).
[25] J. Mclean and P. G. Saffman, J. Fluid Mech. **102**, 455 (1981).
[26] J. J. Xu, Eur. J. Appl. Math. **2**, 105 (1991).
[27] J. J. Xu, IMA J. Appl. Math. **57**, 101 (1996).
[28] J. J. Xu, Eur. J. Appl. Math. **7**, 169 (1996).
[29] I. S. Gradshteyn and I. M. Ryzhik, *Table of Integrals, Series and Products*, 2nd ed. (Academic, New York, 2007).
[30] J. Kevorkian and J. D. Cole, *Multiple Scale and Singular Perturbation Methods*, Applied Mathematical Sciences, Vol. 114 (Springer-Verlag, New York, Heidelberg, Berlin, 1996).
[31] J. J. Xu, *Interfacial Wave Theory of Pattern Formation: Selection of Dendrite Growth and Viscous Fingering in a Hele–Shaw Flow* (Springer-Verlag, Berlin, Heidelberg, New York, 1998).
[32] P. Kurowski, S. de Cheveign, G. Faivre, and C. Guthmann, J. Phys. (France) **50**, 3007 (1989).
[33] K. Brattkus, J. Phys. (France) **50**, 2999 (1989).